

Unitary Fermi gas, ϵ expansion, and nonrelativistic conformal field theories

Yusuke Nishida and Dam Thanh Son

Abstract We review theoretical aspects of unitary Fermi gas (UFG), which has been realized in ultracold atom experiments. We first introduce the ϵ expansion technique based on a systematic expansion in terms of the dimensionality of space. We apply this technique to compute the thermodynamic quantities, the quasiparticle spectrum, and the critical temperature of UFG. We then discuss consequences of the scale and conformal invariance of UFG. We prove a correspondence between primary operators in nonrelativistic conformal field theories and energy eigenstates in a harmonic potential. We use this correspondence to compute energies of fermions at unitarity in a harmonic potential. The scale and conformal invariance together with the general coordinate invariance constrains the properties of UFG. We show the vanishing bulk viscosities of UFG and derive the low-energy effective Lagrangian for the superfluid UFG. Finally we propose other systems exhibiting the nonrelativistic scaling and conformal symmetries that can be in principle realized in ultracold atom experiments.

Yusuke Nishida
Center for Theoretical Physics, Massachusetts Institute of Technology
Cambridge, Massachusetts 02139, USA; e-mail: nishida@mit.edu

Dam Thanh Son
Institute for Nuclear Theory, University of Washington
Seattle, Washington 98195, USA; e-mail: son@phys.washington.edu

1	Introduction	3
2	ϵ expansion for the unitary Fermi gas	5
	2.1 Why four and two spatial dimensions are special?	6
	2.1.1 Nussinovs' intuitive arguments	6
	2.1.2 Field theoretical approach	6
	2.2 Feynman rules and power counting of ϵ	8
	2.2.1 Around four spatial dimensions	8
	2.2.2 Around two spatial dimensions	10
	2.3 Zero temperature thermodynamics	11
	2.3.1 Next-to-leading orders	12
	2.3.2 Next-to-next-to-leading orders	15
	2.4 Quasiparticle spectrum	16
	2.5 Critical temperature	17
	2.6 Phase diagram of an imbalanced Fermi gas	20
3	Aspects as a nonrelativistic conformal field theory	20
	3.1 Schrödinger algebra	20
	3.2 Operator-state correspondence	22
	3.2.1 Primary operators	22
	3.2.2 Correspondence to states in a harmonic potential	23
	3.2.3 Unitarity bound of scaling dimensions	25
	3.2.4 Nonuniversality of p -wave resonances	26
	3.3 Scaling dimensions of composite operators	26
	3.3.1 Two-body operator	27
	3.3.2 Three-body operators	27
	3.4 Application of the ϵ expansion	29
	3.4.1 Scaling dimensions near four spatial dimensions	29
	3.4.2 Scaling dimensions near two spatial dimensions	31
	3.4.3 Interpolations of ϵ expansions	32
4	General coordinate and conformal invariance	34
	4.1 Vanishing bulk viscosities	36
	4.1.1 Normal phase	36
	4.1.2 Superfluid phase	38
	4.2 Superfluid effective field theory	39
5	Other scale and conformal invariant systems	40
6	Appendix: scaling dimensions of three-body operators	41
	References	42

1 Introduction

Interacting fermions appear in various subfields of physics. The Bardeen-Cooper-Schrieffer (BCS) mechanism shows that if the interaction is attractive, the Fermi surface is unstable toward the formation of Cooper pairs and the ground state of the system exhibits superconductivity or superfluidity. Such phenomena have been observed in metallic superconductors, superfluid ^3He , and high- T_c superconductors. Possibilities of superfluid nuclear matter, color superconductivity of quarks, and neutrino superfluidity are also discussed in literatures; some of these states might be important to the physics of neutron stars.

In 2004, a new type of fermionic superfluid has been realized in ultracold atomic gases of ^{40}K and ^6Li in optical traps [1, 2]. Unlike the previous examples, these systems have a remarkable feature that the strength of the attraction between fermions can be arbitrarily tuned through magnetic field induced Feshbach resonances. The interatomic interaction at ultracold temperature is dominated by binary s -wave collisions, whose strength is characterized by the s -wave scattering length a . Across the Feshbach resonance, a^{-1} can, in principle, be tuned to any value from $-\infty$ to $+\infty$. Therefore, the ultracold atomic gases provide an ideal ground for studying quantum physics of interacting fermions from weak coupling to strong coupling.

In cold and dilute atomic gases, the interatomic potential is well approximated by a zero-range contact interaction: the potential range, $r_0 \sim 60a_0$ for ^{40}K and $r_0 \sim 30a_0$ for ^6Li , is negligible compared to the de Broglie wavelength and the mean interparticle distance ($n^{-1/3} \sim 5000\text{-}10000a_0$). The properties of such a system are *universal*, i.e., independent of details of the interaction potential. By regarding the two different hyperfine states of fermionic atoms as spin- \uparrow and spin- \downarrow fermions, the atomic gas reduces to a gas of spin- $\frac{1}{2}$ fermions interacting by the zero-range potential with the tunable scattering length a . The question we would like to understand is the phase diagram of such a system as a function of the dimensionless parameter $-\infty < (ak_F)^{-1} < \infty$, where $k_F \equiv (3\pi^2n)^{1/3}$ is the Fermi momentum.

The qualitative understanding of the phase diagram is provided by picture of a BCS-BEC crossover [3, 4, 5] (the horizontal axis in Fig. 1). When the attraction between fermions is weak (BCS limit where $ak_F < 0$ and $|ak_F| \ll 1$), the system is a weakly interacting Fermi gas. Its ground state is superfluid by the BCS mechanism, where (loosely bound) Cooper pairs condense. On the other hand, when the attraction is strong (BEC limit where $0 < ak_F \ll 1$), two fermions form a bound molecule and the system becomes a weakly interacting Bose gas of such molecules. Its ground state again exhibits superfluidity, but by the Bose-Einstein condensation (BEC) of the tightly bound molecules. These two regimes are smoothly connected without phase transitions, which implies that the ground state of the system is a superfluid for any $(ak_F)^{-1}$. Both BCS and BEC limits can be understood quantitatively by using the standard perturbative expansion in terms of the small parameter $|ak_F| \ll 1$.

In contrast, a strongly interacting regime exists in the middle of the BCS-BEC crossover, where the scattering length is comparable to or exceeds the mean interparticle distance; $|ak_F| \gtrsim 1$. In particular, the limit of infinite scattering length

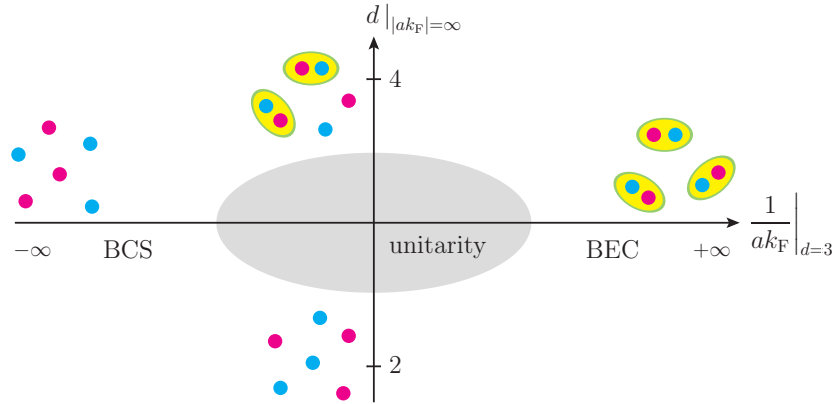


Fig. 1 Extended phase diagram of the BCS-BEC crossover in the plane of the inverse scattering length $(ak_F)^{-1}$ and the spatial dimension d . There are four limits where the system becomes noninteracting; $ak_F \rightarrow \pm\infty$ and $d \rightarrow 4, 2$. The system is strongly interacting in the shaded region.

$|ak_F| \rightarrow \infty$, which is often called the *unitarity* limit, has attracted intense attention by experimentalists and theorists alike. Beside being experimentally realizable in ultracold atomic gases using the Feshbach resonance, this regime is an idealization of the dilute nuclear matter, where the neutron-neutron scattering length $a_{nn} \simeq -18.5$ fm is larger than the typical range of the nuclear force $r_0 \simeq 1.4$ fm.

Theoretical treatments of the Fermi gas in the unitarity limit (unitary Fermi gas) suffer from the difficulty arising from the lack of a small expansion parameter: the standard perturbative expansion in terms of $|ak_F|$ is obviously of no use. Mean-field type approximations, with or without fluctuations, are often adopted to obtain a qualitative understanding of the BCS-BEC crossover, but they are not necessarily controlled near the unitarity limit. Therefore an important and challenging problem for theorists is to establish a *systematic* approach to investigate the unitary Fermi gas.

In Sect. 2 of this chapter we describe one of such approaches. It is based on an expansion over a parameter which depends on the dimensionality of space [6, 7, 8]. In this approach, one extends the problem to arbitrary spatial dimension d , keeping the scattering length infinite $|ak_F| \rightarrow \infty$ (the vertical axis in Fig. 1). Then we can find two noninteracting limits on the d axis, which are $d = 4$ and $d = 2$. Accordingly, slightly below four or slightly above two spatial dimensions, the unitary Fermi gas becomes weakly interacting and thus a “perturbative expansion” is available. We show that the unitary Fermi gas near $d = 4$ is described by a weakly interacting gas of bosons and fermions, while near $d = 2$ it reduces to a weakly interacting Fermi gas. A small parameter for the perturbative expansion is $\epsilon \equiv 4 - d$ near four spatial dimensions or $\bar{\epsilon} \equiv d - 2$ near two spatial dimensions. After performing all calculations treating ϵ or $\bar{\epsilon}$ as a small expansion parameter, results for the physical case of $d = 3$ are obtained by extrapolating the series expansions to $\epsilon(\bar{\epsilon}) = 1$, or more

appropriately, by matching the two series expansions. We apply this technique, the ϵ expansion, to compute the thermodynamic quantities [6, 7, 9, 10] (Sect. 2.3), the quasiparticle spectrum [6, 7] (Sect. 2.4), and the critical temperature [8] (Sect. 2.5). The main advantage of this method is that all calculations can be done analytically; its drawback is that interpolations to $d = 3$ are needed to achieve numerical accuracy.

Then in Sects. 3 and 4, we focus on consequences of another important characteristic of the unitary Fermi gas, namely, the scale and conformal invariance [11, 12, 13]. We introduce the notion of nonrelativistic conformal field theories (NRCFTs) as theories describing nonrelativistic systems exhibiting the scaling and conformal symmetries. In Sect. 3.1, we describe a nonrelativistic analog of the conformal algebra, the so-called Schrödinger algebra [14, 15], and show in Sect. 3.2 that there is an operator-state correspondence [11]: a primary operator in NRCFT corresponds to an energy eigenstate of a few-particle system in a harmonic potential. The scaling dimension of the primary operator coincides with the energy eigenvalue of the corresponding state, divided by the oscillator frequency. We use the operator-state correspondence to compute the energies of two and three fermions at unitarity in a harmonic potential exactly (Sect. 3.3 with Appendix) and more fermions with the help of the ϵ expansion (Sect. 3.4).

The enlarged symmetries of the unitary Fermi gas also constrain its properties. By requiring the scale and conformal invariance and the general coordinate invariance of the hydrodynamic equations, we show that the unitary Fermi gas has the vanishing bulk viscosity in the normal phase [12] (Sect. 4.1). In the superfluid phase, two of the three bulk viscosities have to vanish while the third one is allowed to be nonzero. In Sect. 4.2, we derive the most general effective Lagrangian for the superfluid unitary Fermi gas that is consistent with the scale, conformal, and general coordinate invariance in the systematic momentum expansion [13]. To the leading and next-to-leading orders, there are three low-energy constants which can be computed using the ϵ expansion. We can express various physical quantities through these constants.

Finally in Sect. 5, we discuss other systems exhibiting the nonrelativistic scaling and conformal symmetries, to which a part of above results can be applied. Such systems include a mass-imbalanced Fermi gas with both two-body and three-body resonances [16] and Fermi gases in mixed dimensions [17]. These systems can be in principle realized in ultracold atom experiments.

2 ϵ expansion for the unitary Fermi gas

In this section, we develop an analytical approach for the unitary Fermi gas based on a systematic expansion in terms of the dimensionality of space by using special features of four or two spatial dimensions for the zero-range and infinite scattering length interaction.

2.1 Why four and two spatial dimensions are special?

2.1.1 Nussinov's intuitive arguments

The special role of four and two spatial dimensions for the zero-range and infinite scattering length interaction has been first recognized by Nussinov and Nussinov [18]. At infinite scattering length, which corresponds to a resonance at zero energy, the two-body wave function at a short distance $r \rightarrow 0$ behaves like

$$R(r) \propto \frac{1}{r^{d-2}} + O(r^{4-d}), \quad (1)$$

where r is the separation between two fermions with opposite spins. The first singular term $\sim 1/r^{d-2}$ is the spherically symmetric solution to the Laplace equation in d spatial dimensions. Accordingly the normalization integral of the wave function has the form

$$\int dr R(r)^2 \propto \int_0^\infty dr \frac{1}{r^{d-3}}, \quad (2)$$

which diverges at the origin $r \rightarrow 0$ in higher dimensions $d \geq 4$. Therefore, in the limit $d \rightarrow 4$, the two-body wave function is concentrated at the origin and the fermion pair should behave like a point-like composite boson. This observation led Nussinov and Nussinov to conclude that the unitary Fermi gas at $d \rightarrow 4$ becomes a noninteracting Bose gas.

On the other hand, the singularity in the wave function (1) disappears in the limit $d \rightarrow 2$, which means that the interaction between the two fermions also disappears. This can be understood intuitively from the fact that in lower dimensions $d \leq 2$, any attractive potential possesses at least one bound state and thus the threshold of the appearance of the first bound state (infinite scattering length) corresponds to the vanishing potential. Therefore the unitary Fermi gas at $d \rightarrow 2$ should reduce to a noninteracting Fermi gas [18].

The physical case, $d = 3$, lies midway between these two limits $d = 2$ and $d = 4$. It seems natural to try to develop an expansion around these two limits and then extrapolate to $d = 3$. For this purpose, we need to employ a field theoretical approach.

2.1.2 Field theoretical approach

Spin- $\frac{1}{2}$ fermions interacting by the zero-range potential is described by the following Lagrangian density (here and below $\hbar = k_B = 1$):

$$\mathcal{L} = \sum_{\sigma=\uparrow,\downarrow} \psi_\sigma^\dagger \left(i\partial_t + \frac{\partial^2}{2m} + \mu \right) \psi_\sigma + c_0 \psi_\uparrow^\dagger \psi_\downarrow^\dagger \psi_\downarrow \psi_\uparrow. \quad (3)$$

In $d = 3$, the bare coupling c_0 is related to the physical parameter, the scattering length a , by

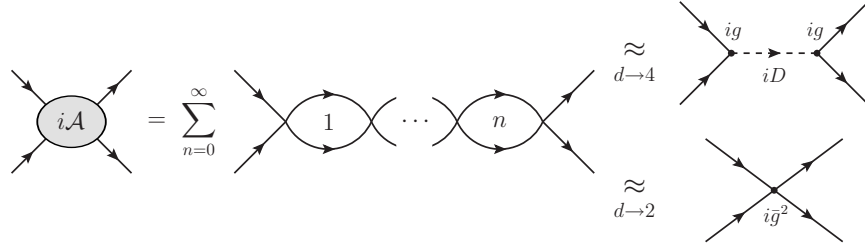


Fig. 2 Two-fermion scattering in vacuum in the unitarity limit. The scattering amplitude $i\mathcal{A}$ near $d = 4$ is expressed by the propagation of a boson with the small effective coupling g , while it reduces to a contact interaction with the small effective coupling \bar{g}^2 near $d = 2$.

$$\frac{1}{c_0} = -\frac{m}{4\pi a} + \int \frac{d\mathbf{k}}{(2\pi)^d} \frac{1}{2\epsilon_{\mathbf{k}}} \quad \left(\epsilon_{\mathbf{k}} \equiv \frac{\mathbf{k}^2}{2m} \right). \quad (4)$$

In dimensional regularization, used in this section, the second term vanishes and therefore the unitarity limit $a \rightarrow \infty$ corresponds to $c_0 \rightarrow \infty$.

In order to understand the specialty of $d = 4$ and $d = 2$, we first study the scattering of two fermions in vacuum ($\mu = 0$) in general d spatial dimensions. The two-body scattering amplitude $i\mathcal{A}$ is given by the geometric series of bubble diagrams depicted in Fig. 2. In the unitarity limit, we obtain

$$i\mathcal{A}(p_0, \mathbf{p}) = -i \frac{\left(\frac{4\pi}{m}\right)^{d/2}}{\Gamma\left(1 - \frac{d}{2}\right) \left(-p_0 + \frac{\epsilon_{\mathbf{p}}}{2} - i0^+\right)^{d/2-1}}, \quad (5)$$

which vanishes when $d \rightarrow 4$ and $d \rightarrow 2$ because of the poles in $\Gamma\left(1 - \frac{d}{2}\right)$. This means that those dimensions correspond to the noninteracting limits and is consistent with the Nussinovs' arguments in Sect. 2.1.1.

Furthermore, by expanding $i\mathcal{A}$ in terms of $\epsilon = 4 - d \ll 1$, we can obtain further insight. The scattering amplitude to the leading order in ϵ becomes

$$\begin{aligned} i\mathcal{A}(p_0, \mathbf{p}) &= -\frac{8\pi^2\epsilon}{m^2} \frac{i}{p_0 - \frac{\epsilon_{\mathbf{p}}}{2} + i0^+} + O(\epsilon^2) \\ &\equiv (ig)^2 iD(p_0, \mathbf{p}) + O(\epsilon^2), \end{aligned} \quad (6)$$

where we have defined $g^2 = \frac{8\pi^2\epsilon}{m^2}$ and $D(p_0, \mathbf{p}) = \left(p_0 - \frac{\epsilon_{\mathbf{p}}}{2} + i0^+\right)^{-1}$. The latter is the propagator of a particle of mass $2m$. This particle is a boson, which is the point-like composite of two fermions. Equation (6) states that the two-fermion scattering near $d = 4$ can be thought of as occurring through the propagation of an intermediate boson, as depicted in Fig. 2. The effective coupling of the two fermions with the boson is $g \sim \epsilon^{1/2}$, which becomes small near $d = 4$. This indicates the possibility to formulate a systematic perturbative expansion for the unitary Fermi gas around $d = 4$ as a weakly interacting fermions and bosons.

Similarly, by expanding $i\mathcal{A}$ in $\bar{\epsilon} = d - 2 \ll 1$, the scattering amplitude becomes

$$i\mathcal{A}(p_0, \mathbf{p}) = i\frac{2\pi}{m}\bar{\epsilon} + O(\bar{\epsilon}^2) \equiv i\bar{g}^2 + O(\bar{\epsilon}^2), \quad (7)$$

where we have defined $\bar{g}^2 = \frac{2\pi}{m}\bar{\epsilon}$. Equation (7) shows that the two-fermion scattering near $d = 2$ reduces to that caused by a contact interaction with the effective coupling \bar{g}^2 (Fig. 2). Because $\bar{g}^2 \sim \bar{\epsilon}$ is small near $d = 2$, it will be possible to formulate another systematic perturbative expansion for the unitary Fermi gas around $d = 2$ as a weakly interacting fermions.

2.2 Feynman rules and power counting of ϵ

The observations in Sect. 2.1.2 reveal how we should construct the systematic expansions for the unitary Fermi gas around $d = 4$ and $d = 2$. Here we provide their formulations and power counting rules of ϵ ($\bar{\epsilon}$). The detailed derivations of the power counting rules can be found in Ref. [7].

2.2.1 Around four spatial dimensions

In order to organize a systematic expansion around $d = 4$, we make a Hubbard-Stratonovich transformation and rewrite the Lagrangian density (3) as

$$\mathcal{L} \rightarrow \sum_{\sigma=\uparrow,\downarrow} \psi_\sigma^\dagger \left(i\partial_t + \frac{\partial^2}{2m} + \mu \right) \psi_\sigma - \frac{1}{c_0} \phi^\dagger \phi + \psi_\uparrow^\dagger \psi_\downarrow^\dagger \phi + \phi^\dagger \psi_\downarrow \psi_\uparrow \quad (8a)$$

$$= \Psi^\dagger \left(i\partial_t + \sigma_3 \frac{\partial^2}{2m} + \sigma_3 \mu \right) \Psi - \frac{1}{c_0} \phi^\dagger \phi + \Psi^\dagger \sigma_+ \Psi \phi + \phi^\dagger \Psi^\dagger \sigma_- \Psi, \quad (8b)$$

where $\Psi \equiv (\psi_\uparrow, \psi_\downarrow)^T$ is a two-component Nambu-Gor'kov field, $\sigma_\pm \equiv \frac{1}{2}(\sigma_1 \pm i\sigma_2)$, and $\sigma_{1,2,3}$ are the Pauli matrices. Because the ground state of the system at finite density is a superfluid, we expand ϕ around its vacuum expectation value $\phi_0 \equiv \langle \phi \rangle > 0$ as

$$\phi = \phi_0 + g\varphi \quad \text{with} \quad g \equiv \frac{(8\pi^2\epsilon)^{1/2}}{m} \left(\frac{m\phi_0}{2\pi} \right)^{\epsilon/4}. \quad (9)$$

Here we introduced the effective coupling g and chose the extra factor $(m\phi_0/2\pi)^{\epsilon/4}$ so that φ has the same dimension as a nonrelativistic field.¹

¹ The choice of the extra factor is arbitrary, if it has the correct dimension, and does not affect final results because the difference can be absorbed by the redefinition of φ . The particular choice of g in Eq. (9) [or \bar{g} in Eq. (13)] simplifies expressions for loop integrals in the intermediate steps.

Because the Lagrangian density (8b) does not have the kinetic term for the boson field φ , we add and subtract its kinetic term by hand and rewrite the Lagrangian density as a sum of three parts, $\mathcal{L} = \mathcal{L}_0 + \mathcal{L}_1 + \mathcal{L}_2$, where

$$\mathcal{L}_0 = \Psi^\dagger \left(i\partial_t + \sigma_3 \frac{\partial^2}{2m} + \sigma_1 \phi_0 \right) \Psi + \varphi^\dagger \left(i\partial_t + \frac{\partial^2}{4m} \right) \varphi, \quad (10a)$$

$$\mathcal{L}_1 = g\Psi^\dagger \sigma_+ \Psi \varphi + g\varphi^\dagger \Psi^\dagger \sigma_- \Psi + \mu\Psi^\dagger \sigma_3 \Psi + 2\mu\varphi^\dagger \varphi, \quad (10b)$$

$$\mathcal{L}_2 = -\varphi^\dagger \left(i\partial_t + \frac{\partial^2}{4m} \right) \varphi - 2\mu\varphi^\dagger \varphi. \quad (10c)$$

Here we set $1/c_0 = 0$ in the unitarity limit. We treat \mathcal{L}_0 as the unperturbed part and \mathcal{L}_1 as a small perturbation. Note that the chemical potential μ is also treated as a perturbation because we will find it small, $\mu/\phi_0 \sim \epsilon$, by solving the gap equation. Physically, $\mathcal{L}_0 + \mathcal{L}_1$ is the Lagrangian density describing weakly interacting fermions Ψ and bosons φ with a small coupling $g \sim \epsilon^{1/2}$. \mathcal{L}_2 plays a role of counter terms that cancel $1/\epsilon$ singularities of loop integrals in certain types of diagrams (Fig. 3).

The unperturbed part \mathcal{L}_0 generates the fermion propagator,

$$G(p_0, \mathbf{p}) = \frac{1}{p_0^2 - E_{\mathbf{p}}^2 + i0^+} \begin{pmatrix} p_0 + \epsilon_{\mathbf{p}} & -\phi_0 \\ -\phi_0 & p_0 - \epsilon_{\mathbf{p}} \end{pmatrix}, \quad (11)$$

with $E_{\mathbf{p}} \equiv \sqrt{\epsilon_{\mathbf{p}}^2 + \phi_0^2}$ and the boson propagator

$$D(p_0, \mathbf{p}) = \frac{1}{p_0 - \frac{\epsilon_{\mathbf{p}}}{2} + i0^+}. \quad (12)$$

The first two terms in the perturbation part \mathcal{L}_1 generate the fermion-boson vertices whose coupling is g in Eq. (9). The third and fourth terms are the chemical potential insertions to the fermion and boson propagators. The two terms in \mathcal{L}_2 provide additional vertices, $-i\Pi_0$ and $-2i\mu$ in Fig. 3(b) and (d), to the boson propagator, where $\Pi_0(p_0, \mathbf{p}) \equiv p_0 - \frac{\epsilon_{\mathbf{p}}}{2}$.

The power counting rule of ϵ is simple and summarized as follows:

1. We regard ϕ_0 as $O(1)$ and hence $\mu \sim \epsilon\phi_0$ as $O(\epsilon)$.
2. We write down Feynman diagrams for the quantity of interest using the propagators from \mathcal{L}_0 and the vertices from \mathcal{L}_1 .
3. If the written Feynman diagram includes any subdiagram of the type in Fig. 3(a) or Fig. 3(c), we add the same Feynman diagram where the subdiagram is replaced by the vertex from \mathcal{L}_2 in Fig. 3(b) or Fig. 3(d).
4. The power of ϵ for the given Feynman diagram is $O(\epsilon^{N_g/2 + N_\mu})$, where N_g is the number of couplings g and N_μ is the number of chemical potential insertions.
5. The only exception is the one-loop vacuum diagram with one μ insertion (the second diagram in Fig. 5), which is $O(1)$ instead of $O(\epsilon)$ due to the $1/\epsilon$ singularity arising from the loop integral.

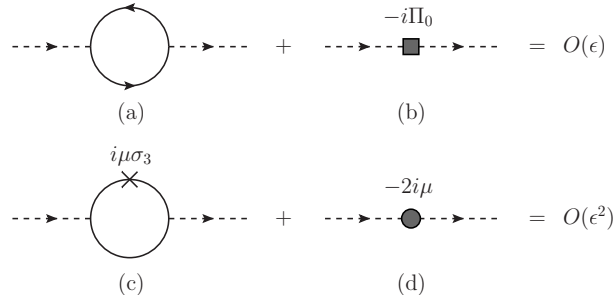


Fig. 3 Power counting rule of ϵ . The $1/\epsilon$ singularity in the boson self-energy diagram (a) or (c) can be canceled by combining it with the vertex from \mathcal{L}_2 , (b) or (d), to achieve the simple ϵ counting. Solid (dotted) lines are the fermion (boson) propagators iG (iD). The fermion loop in (c) goes around clockwise and counterclockwise and the cross symbol represents the μ insertion.

The same or similar power counting rule can be derived for the cases with unequal chemical potentials $\mu_\uparrow \neq \mu_\downarrow$ [7], unequal masses $m_\uparrow \neq m_\downarrow$ [19], at finite temperature $T \neq 0$ [8], and in the vicinity of the unitarity limit $c_0 \neq 0$ [7].

2.2.2 Around two spatial dimensions

The systematic expansion around $d = 2$ in terms of $\bar{\epsilon}$ can be also organized in a similar way. Starting with the Lagrangian density (8b), we expand ϕ around its vacuum expectation value $\bar{\phi}_0 \equiv \langle \phi \rangle > 0$ as

$$\phi = \bar{\phi}_0 + \bar{g}\varphi \quad \text{with} \quad \bar{g} \equiv \left(\frac{2\pi\bar{\epsilon}}{m}\right)^{1/2} \left(\frac{m\mu}{2\pi}\right)^{-\bar{\epsilon}/4}. \quad (13)$$

Here we introduced the effective coupling \bar{g} and chose the extra factor $(m\mu/2\pi)^{-\bar{\epsilon}/4}$ so that $\varphi^\dagger\varphi$ has the same dimension as the Lagrangian density.²

In the unitarity limit $1/c_0 = 0$, we rewrite the Lagrangian density as a sum of three parts, $\mathcal{L} = \bar{\mathcal{L}}_0 + \bar{\mathcal{L}}_1 + \bar{\mathcal{L}}_2$, where

$$\bar{\mathcal{L}}_0 = \Psi^\dagger \left(i\partial_t + \sigma_3 \frac{\partial^2}{2m} + \sigma_3 \mu + \sigma_1 \bar{\phi}_0 \right) \Psi, \quad (14a)$$

$$\bar{\mathcal{L}}_1 = -\varphi^\dagger \varphi + \bar{g}\Psi^\dagger \sigma_+ \Psi \varphi + \bar{g}\varphi^\dagger \Psi^\dagger \sigma_- \Psi, \quad (14b)$$

$$\bar{\mathcal{L}}_2 = \varphi^\dagger \varphi. \quad (14c)$$

We treat $\bar{\mathcal{L}}_0$ as the unperturbed part and $\bar{\mathcal{L}}_1$ as a small perturbation. Physically, $\bar{\mathcal{L}}_0 + \bar{\mathcal{L}}_1$ is the Lagrangian density describing weakly interacting fermions Ψ . Indeed, if we did not have $\bar{\mathcal{L}}_2$, we could integrate out the auxiliary fields φ and φ^\dagger ,

² See the footnote after Eq. (9).

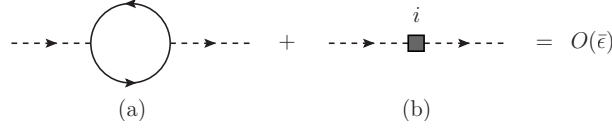


Fig. 4 Power counting rule of $\bar{\epsilon}$. The $1/\bar{\epsilon}$ singularity in the self-energy diagram of ϕ field (a) can be canceled by combining it with the vertex from $\tilde{\mathcal{L}}_2$ (b) to achieve the simple $\bar{\epsilon}$ counting. Solid (dotted) lines are the fermion (auxiliary field) propagators $i\tilde{G}$ ($i\tilde{D}$).

$$\tilde{\mathcal{L}}_1 \rightarrow \bar{g}^2 \Psi^\dagger \sigma_+ \Psi \Psi^\dagger \sigma_- \Psi = \bar{g}^2 \psi_\uparrow^\dagger \psi_\downarrow^\dagger \psi_\downarrow \psi_\uparrow, \quad (15)$$

which is the contact interaction between fermions with a small coupling $\bar{g}^2 \sim \bar{\epsilon}$. $\tilde{\mathcal{L}}_2$ plays a role of a counter term that cancels $1/\bar{\epsilon}$ singularities of loop integrals in a certain type of diagrams (Fig. 4).

The unperturbed part $\tilde{\mathcal{L}}_0$ generates the fermion propagator

$$\tilde{G}(p_0, \mathbf{p}) = \frac{1}{p_0^2 - \bar{E}_p^2 + i0^+} \begin{pmatrix} p_0 + \epsilon_p - \mu & -\bar{\phi}_0 \\ -\bar{\phi}_0 & p_0 - \epsilon_p + \mu \end{pmatrix} \quad (16)$$

with $\bar{E}_p \equiv \sqrt{(\epsilon_p - \mu)^2 + \bar{\phi}_0^2}$. The first term in the perturbation part $\tilde{\mathcal{L}}_1$ generates the propagator of ϕ field, $\tilde{D}(p_0, \mathbf{p}) = -1$, and the last two terms generate the vertices between fermions and ϕ field with the coupling \bar{g} in Eq. (13). $\tilde{\mathcal{L}}_2$ provides an additional vertex i in Fig. 4(b) to the ϕ propagator.

The power counting rule of $\bar{\epsilon}$ is simple and summarized as follows:

1. We regard μ as $O(1)$.
2. We write down Feynman diagrams for the quantity of interest using the propagator from $\tilde{\mathcal{L}}_0$ and the vertices from $\tilde{\mathcal{L}}_1$.
3. If the written Feynman diagram includes any subdiagram of the type in Fig. 4(a), we add the same Feynman diagram where the subdiagram is replaced by the vertex from $\tilde{\mathcal{L}}_2$ in Fig. 4(b).
4. The power of $\bar{\epsilon}$ for the given Feynman diagram is $O(\bar{\epsilon}^{N_{\bar{g}}/2})$, where $N_{\bar{g}}$ is the number of couplings \bar{g} .

2.3 Zero temperature thermodynamics

We now apply the developed ϵ expansion to compute various physical quantities of the unitary Fermi gas. Because of the absence of scales in the zero-range and infinite scattering interaction, the density n is the only scale of the unitary Fermi gas at zero temperature. Therefore all physical quantities are determined by simple dimensional analysis up to dimensionless constants of proportionality. Such dimensionless parameters are universal depending only on the dimensionality of space.

$$V_{\text{eff}} = \text{[circle with arrow]} + \text{[circle with arrow and cross]} + \text{[circle with arrow and dashed line]} + O(\epsilon^2)$$

$O(1)$ $O(1)$ $O(\epsilon)$

Fig. 5 Vacuum diagrams contributing to the effective potential near $d = 4$ to leading and next-to-leading orders in ϵ . The boson one-loop diagram vanishes at zero temperature.

A representative example of the universal parameters is the ground state energy of the unitary Fermi gas normalized by that of a noninteracting Fermi gas with the same density:

$$\xi \equiv \frac{E_{\text{unitary}}}{E_{\text{free}}}. \quad (17)$$

ξ , sometimes called the Bertsch parameter, measures how much energy is gained due to the attractive interaction in the unitarity limit. In terms of ξ , the pressure P , the energy density \mathcal{E} , the chemical potential μ , and the sound velocity v_s of the unitary Fermi gas are given by

$$\frac{P}{\epsilon_F n} = \frac{2}{d+2} \xi, \quad \frac{\mathcal{E}}{\epsilon_F n} = \frac{d}{d+2} \xi, \quad \frac{\mu}{\epsilon_F} = \xi, \quad \frac{v_s}{v_F} = \sqrt{\frac{\xi}{d}}, \quad (18)$$

where $\epsilon_F \equiv k_F^2/2m$ and $v_F \equiv k_F/m$ are the Fermi energy and velocity with $k_F \equiv [2^{d-1} \pi^{d/2} \Gamma(\frac{d}{2} + 1) n]^{1/d}$ being the Fermi momentum in d spatial dimensions. ξ is thus a fundamental quantity characterizing the zero temperature thermodynamics of the unitary Fermi gas.

2.3.1 Next-to-leading orders

ξ can be determined systematically in the ϵ expansion by computing the effective potential $V_{\text{eff}}(\phi_0)$, whose minimum with respect to the order parameter ϕ_0 provides the pressure $P = -\min V_{\text{eff}}(\phi_0)$. To leading and next-to-leading orders in ϵ , the effective potential receives contributions from three vacuum diagrams depicted in Fig. 5. The third diagram, fermion loop with one boson exchange, results from the summation of fluctuations around the classical solution and is beyond the mean field approximation. Any other diagrams are suppressed near $d = 4$ by further powers of ϵ . Performing the loop integrations, we obtain

$$V_{\text{eff}}(\phi_0) = \left[\frac{\phi_0}{3} \left\{ 1 + \frac{7-3(\gamma+\ln 2)}{6} \epsilon - 3C\epsilon \right\} - \frac{\mu}{\epsilon} \left\{ 1 + \frac{1-2(\gamma-\ln 2)}{4} \epsilon \right\} \right] \left(\frac{m\phi_0}{2\pi} \right)^{d/2} + O(\epsilon^2), \quad (19)$$

$$\bar{V}_{\text{eff}} = \begin{array}{c} \text{---} \circlearrowleft \text{---} \\ O(1) \end{array} + \begin{array}{c} \text{---} \circlearrowleft \text{---} \\ \text{---} \text{---} \text{---} \\ O(\bar{\epsilon}) \end{array} + O(\bar{\epsilon}^2)$$

Fig. 6 Vacuum diagrams contributing to the effective potential near $d = 2$ to leading and next-to-leading orders in $\bar{\epsilon}$.

where $C \approx 0.14424$ is a numerical constant. The minimization of $V_{\text{eff}}(\phi_0)$ with respect to ϕ_0 gives the gap equation, $\partial V_{\text{eff}}/\partial \phi_0 = 0$, which is solved by

$$\phi_0(\mu) = \frac{2\mu}{\epsilon} [1 + (3C - 1 + \ln 2)\epsilon + O(\epsilon^2)]. \quad (20)$$

The effective potential at its minimum provides the pressure $P(\mu) = -V_{\text{eff}}(\phi_0(\mu))$ as a function of μ . From Eq. (18) and $n = \partial P/\partial \mu$, we obtain ξ expanded in terms of ϵ :

$$\begin{aligned} \xi|_{d \rightarrow 4} &= \frac{\epsilon^{3/2}}{2} \exp\left(\frac{\epsilon \ln \epsilon}{8 - 2\epsilon}\right) \left[1 - \left\{3C - \frac{5}{4}(1 - \ln 2)\right\}\epsilon + O(\epsilon^2)\right] \\ &= \frac{1}{2}\epsilon^{3/2} + \frac{1}{16}\epsilon^{5/2} \ln \epsilon - 0.0246\epsilon^{5/2} + O(\epsilon^{7/2}). \end{aligned} \quad (21)$$

Although our formalism is based on the smallness of ϵ , we find that the next-to-leading-order correction is quite small compared to the leading term even at $\epsilon = 1$. The naive extrapolation to the physical dimension $d = 3$ gives

$$\xi \rightarrow 0.475 \quad (\epsilon \rightarrow 1), \quad (22)$$

which is already close to the result from the Monte Carlo simulation $\xi \approx 0.40(1)$ [20]. For comparison, the mean field approximation yields $\xi \approx 0.591$.

The above result can be further improved by incorporating the expansion around $d = 2$. Because we can find by solving the gap equation that the order parameter is exponentially small [7]

$$\bar{\phi}_0(\mu) = 2\mu e^{-1/\bar{\epsilon} - 1 + O(\bar{\epsilon})}, \quad (23)$$

its contribution to the pressure is negligible compared to any powers of $\bar{\epsilon}$. To leading and next-to-leading orders in $\bar{\epsilon}$, the effective potential receives contributions from two vacuum diagrams depicted in Fig. 6. Any other diagrams are suppressed near $d = 2$ by further powers of $\bar{\epsilon}$. From the pressure

$$P = -\bar{V}_{\text{eff}}(0) = [1 + \bar{\epsilon} + O(\bar{\epsilon}^2)] \frac{2\mu}{\Gamma(\frac{d}{2} + 2)} \left(\frac{m\mu}{2\pi}\right)^{d/2}, \quad (24)$$

we obtain ξ expanded in terms of $\bar{\epsilon}$:

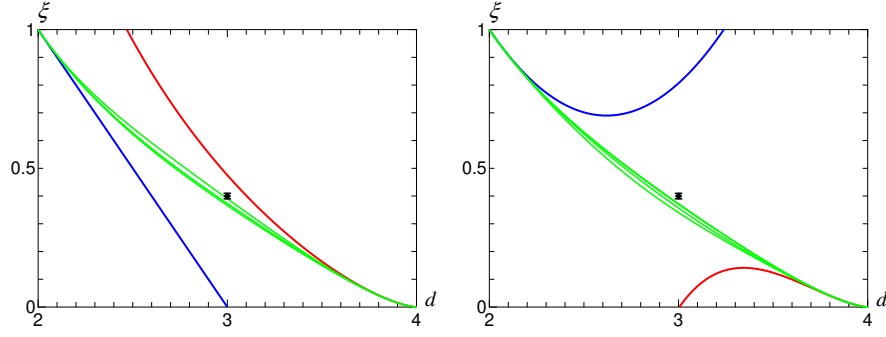


Fig. 7 ξ as a function of the spatial dimension d . Left panel: The upper (lower) curve is the extrapolation from the NLO expansion around $d = 4$ in Eq. (21) [$d = 2$ in Eq. (25)]. The middle three curves show the Padé interpolations of the two NLO expansions. The symbol at $d = 3$ indicates the result $\xi \approx 0.40(1)$ from the Monte Carlo simulation [20]. Right panel: The same as the left panel but including the NNLO corrections in Eqs. (29) and (30).

$$\xi|_{d \rightarrow 2} = 1 - \bar{\epsilon} + O(\bar{\epsilon}^2). \quad (25)$$

The value of ξ in $d = 3$ can be extracted by interpolating the two expansions around $d = 4$ and $d = 2$. The simplest way to do so is to employ the Padé approximants. We write ξ in the form

$$\xi = \frac{\epsilon^{3/2}}{2} \exp\left(\frac{\epsilon \ln \epsilon}{8 - 2\epsilon}\right) F(\epsilon), \quad (26)$$

where $F(\epsilon)$ is an unknown function and the trivial nonanalytic dependence on ϵ was factored out.³ We approximate $F(\epsilon)$ by ratios of two polynomials (Padé approximants) and determine their coefficients so that ξ in Eq. (26) has the correct next-to-leading-order (NLO) expansions both around $d = 4$ [Eq. (21)] and $d = 2$ [Eq. (25)]. The left panel of Fig. 7 shows the behavior of ξ as a function of d . The middle three curves are the Padé interpolations of the two NLO expansions. In $d = 3$, these interpolations give

$$\xi \approx 0.391, 0.366, 0.373, \quad (27)$$

which span a small interval $\xi \approx 0.377 \pm 0.014$.

We can also employ different interpolation schemes, for example, by applying the Borel transformation to $F(\epsilon) = \frac{1}{\epsilon} \int_0^\infty dt e^{-t/\epsilon} G(t)$ and approximating the Borel transform $G(t)$ by the Padé approximants [7]. These Borel-Padé interpolations of the two NLO expansions give

³ It has been shown that $F(\epsilon)$ has a nonanalytic term $-\frac{3}{8}\epsilon^3 \ln \epsilon$ to the next-to-next-to-next-to-leading order in ϵ [9]. Because we are working up to $O(\epsilon^2)$, we neglect such a nonanalytic contribution.

$$\xi \approx 0.391, 0.364, 0.378 \quad (28)$$

in $d = 3$, which again span a small interval $\xi \approx 0.378 \pm 0.013$. Comparing the results in Eqs. (27) and (28), we find that the interpolated values do not depend much on the choice of the Padé approximants and also on the employment of the Borel transformation.

2.3.2 Next-to-next-to-leading orders

The systematic calculation of ξ has been carried out up to the next-to-next-to-leading-order (NNLO) corrections in terms of ϵ [9]:

$$\xi|_{d \rightarrow 4} = \frac{\epsilon^{3/2}}{2} \exp\left(\frac{\epsilon \ln \epsilon}{8 - 2\epsilon}\right) [1 - 0.04916\epsilon - 0.95961\epsilon^2 + O(\epsilon^3)] \quad (29)$$

and in terms of $\bar{\epsilon}$ [10, 19]:

$$\xi|_{d \rightarrow 2} = 1 - \bar{\epsilon} + 0.80685\bar{\epsilon}^2 + O(\bar{\epsilon}^3). \quad (30)$$

The middle four curves in the right panel of Fig. 7 are the Padé interpolations of the two NNLO expansions. In $d = 3$, these interpolations give

$$\xi \approx 0.340, 0.372, 0.370, 0.357, \quad (31)$$

which span an interval $\xi \approx 0.360 \pm 0.020$.⁴ In spite of the large NNLO corrections both near $d = 4$ and $d = 2$, the interpolated values are roughly consistent with the previous interpolations of the NLO expansions (compare the two panels in Fig. 7). This indicates that the interpolated results are stable to inclusion of higher-order corrections and thus the ϵ expansion has a certain predictive power even in the absence of the knowledge on the higher-order corrections.

Finally we note that the limit $\xi|_{d \rightarrow 4} \rightarrow 0$ is consistent with the Nussinovs' picture of the unitary Fermi gas as a noninteracting Bose gas and $\xi|_{d \rightarrow 2} \rightarrow 1$ is consistent with the picture as a noninteracting Fermi gas in Sect. 2.1.1. It would be interesting to consider how ξ should be continued down to $d \rightarrow 1$. The unitary Fermi gas in $d = 3$ is analytically continued to spin- $\frac{1}{2}$ fermions with a hard-core repulsion in $d = 1$, which is equivalent for the thermodynamic quantities to free identical fermions with the same total density [21]. Therefore it is easy to find

$$\xi|_{d \rightarrow 1} \rightarrow 4. \quad (32)$$

The incorporation of this constraint on the Padé interpolations of the two NNLO expansions yields $\xi \approx 0.365 \pm 0.010$ in $d = 3$.

⁴ If we excluded the interpolation by the simple polynomial ($\xi \approx 0.340$) as was done in Ref. [9], we would obtain 0.367 ± 0.010 , which is consistent with the Borel-Padé interpolations without the NNLO correction near $d = 2$ [9].

$$\begin{aligned}
i\mu\sigma_3 &= \longrightarrow \times \longrightarrow \\
-i\Sigma &= \longrightarrow \overset{\curvearrowright}{\text{---}} \longrightarrow + \longrightarrow \overset{\curvearrowleft}{\text{---}} \longrightarrow + O(\epsilon^2)
\end{aligned}$$

Fig. 8 Fermion self-energy diagrams near $d = 4$ to the order $O(\epsilon)$.

2.4 Quasiparticle spectrum

The ϵ expansion is also useful to compute other physical quantities of the unitary Fermi gas. Here we determine the spectrum of fermion quasiparticles in a superfluid. To leading order in ϵ , the dispersion relation $\omega(\mathbf{p})$ is given by the pole of the fermion propagator in Eq. (11); $\omega(\mathbf{p}) = E_{\mathbf{p}} = \sqrt{\epsilon_{\mathbf{p}}^2 + \phi_0^2}$. It has a minimum at $|\mathbf{p}| = 0$ with the energy gap equal to $\Delta = \phi_0 = 2\mu/\epsilon$.

To the next-to-leading order in ϵ , the fermion propagator receives corrections from three self-energy diagrams depicted in Fig. 8. We can find that $\Sigma \sim O(\epsilon)$ is diagonal with the elements

$$\Sigma_{11}(p_0, \mathbf{p}) = -\frac{g^2}{2} \int \frac{d\mathbf{k}}{(2\pi)^d} \frac{E_{\mathbf{k}} - \epsilon_{\mathbf{k}}}{E_{\mathbf{k}}(E_{\mathbf{k}} + \frac{\epsilon_{\mathbf{k}-\mathbf{p}}}{2} - p_0 - i0^+)} \quad (33)$$

and $\Sigma_{22}(p_0, \mathbf{p}) = -\Sigma_{11}(-p_0, -\mathbf{p})$. From the pole of the fermion propagator, $\det[G^{-1}(\omega, \mathbf{p}) + \mu\sigma_3 - \Sigma(\omega, \mathbf{p})] = 0$, we obtain the dispersion relation

$$\omega(\mathbf{p}) = E_{\mathbf{p}} + \frac{\Sigma_{11} + \Sigma_{22}}{2} + \frac{\Sigma_{11} - \Sigma_{22} - 2\mu}{2E_{\mathbf{p}}} \epsilon_{\mathbf{p}} + O(\epsilon^2), \quad (34)$$

where Σ_{11} and Σ_{22} are evaluated at $p_0 = E_{\mathbf{p}}$.

The minimum of $\omega(\mathbf{p})$ will appear at small momentum $\epsilon_{\mathbf{p}} \sim O(\epsilon)$. By expanding $\omega(\mathbf{p})$ with respect to $\epsilon_{\mathbf{p}}$, we find that the dispersion relation around its minimum has the form

$$\omega(\mathbf{p}) \simeq \Delta + \frac{(\epsilon_{\mathbf{p}} - \epsilon_0)^2}{2\phi_0}. \quad (35)$$

Here Δ is the energy gap of the fermion quasiparticle given by

$$\begin{aligned}
\Delta|_{d \rightarrow 4} &= \phi_0 [1 - (8 \ln 3 - 12 \ln 2) \epsilon + O(\epsilon^2)] \\
&= \frac{2\mu}{\epsilon} [1 + (3C - 1 - 8 \ln 3 + 13 \ln 2) \epsilon + O(\epsilon^2)]. \quad (36)
\end{aligned}$$

The minimum of the dispersion relation is located at $\epsilon_{\mathbf{p}} = \epsilon_0 > 0$ with

$$\epsilon_0|_{d \rightarrow 4} = \mu + \frac{\epsilon\phi_0}{2} + O(\epsilon^2) = 2\mu + O(\epsilon^2), \quad (37)$$

where the solution of the gap equation (20) was substituted to ϕ_0 .

We can see that the next-to-leading-order correction is reasonably small compared to the leading term at least for $\Delta/\mu = 2/\epsilon(1 - 0.345\epsilon)$. The naive extrapolation to the physical dimension $d = 3$ gives

$$\frac{\Delta}{\mu} \rightarrow 1.31 \quad \text{and} \quad \frac{\epsilon_0}{\mu} \rightarrow 2 \quad (\epsilon \rightarrow 1), \quad (38)$$

both of which are quite close to the results from the Monte Carlo simulation $\Delta/\mu \approx 1.2$ and $\epsilon_0/\mu \approx 1.9$ [22]. For comparison, the mean field approximation yields $\Delta/\mu \approx 1.16$ and $\epsilon_0/\mu \approx 1$.

Frequently Δ and ϵ_0 are normalized by the Fermi energy ϵ_F . By multiplying Eqs. (36) and (37) by $\mu/\epsilon_F = \xi$ obtained previously in Eq. (21), we find

$$\frac{\Delta}{\epsilon_F} \rightarrow 0.604 \quad \text{and} \quad \frac{\epsilon_0}{\epsilon_F} \rightarrow 1 \quad (\epsilon \rightarrow 1). \quad (39)$$

For comparison, the Monte Carlo simulation gives $\Delta/\epsilon_F \approx 0.50$ and $\epsilon_0/\epsilon_F \approx 0.8$ [22] and the mean field approximation yields $\Delta/\epsilon_F \approx 0.686$ and $\epsilon_0/\epsilon_F \approx 0.591$.

2.5 Critical temperature

The formulation of the ϵ expansion can be extended to finite temperature $T \neq 0$ by using the imaginary time prescription [8]. Here we determine the critical temperature T_c for the superfluid phase transition of the unitary Fermi gas.

The leading contribution to T_c/ϵ_F in terms of ϵ can be obtained by the following simple argument. In the limit $d \rightarrow 4$, the unitary Fermi gas reduces to a noninteracting fermions and bosons with their chemical potentials μ and 2μ , respectively [see Eq. (10)]. Because the boson's chemical potential vanishes at the BEC critical temperature, the density at $T = T_c$ is given by

$$\begin{aligned} n &= 2 \int \frac{d\mathbf{p}}{(2\pi)^4} [f_F(\epsilon_{\mathbf{p}}) + f_B(\epsilon_{\mathbf{p}}/2)] + O(\epsilon) \\ &= \left[\frac{\pi^2}{6} + \frac{8\pi^2}{6} \right] \left(\frac{mT_c}{2\pi} \right)^2 + O(\epsilon) = \frac{3\pi^2}{2} \left(\frac{mT_c}{2\pi} \right)^2 + O(\epsilon). \end{aligned} \quad (40)$$

Comparing the contributions from Fermi and Bose distributions, we can see that only 8 of 9 fermion pairs form the composite bosons while 1 of 9 fermion pairs is dissociated. With the use of $\epsilon_F \equiv \frac{2\pi}{m} \left[\Gamma\left(\frac{d}{2} + 1\right) \frac{n}{2} \right]^{2/d}$ at $d = 4$, we obtain

$$\frac{T_c}{\epsilon_F} \Big|_{d \rightarrow 4} = \sqrt{\frac{2}{3\pi^2}} + O(\epsilon). \quad (41)$$

$$V_{\text{eff}} = \text{[solid circle with arrow]} + \text{[dashed circle with arrow]} + \text{[solid circle with arrow and dashed line]} + \dots$$

$O(1) \qquad O(1) \qquad O(\epsilon)$

Fig. 9 Three types of diagrams contributing to the effective potential at finite temperature near $d = 4$ to leading and next-to-leading orders in ϵ . Each μ (2μ) insertion to the fermion (boson) line increases the power of ϵ by one. Note that at $T \geq T_c$ where $\phi_0 = 0$, the μ insertion to the first diagram does not produce the $1/\epsilon$ singularity.

In order to compute the $O(\epsilon)$ correction to T_c/ϵ_F , we need to evaluate the effective potential $V_{\text{eff}}(\phi_0)$ at finite temperature. The effective potential to leading order in ϵ is given by the fermion one-loop diagrams with and without one μ insertion and the boson one-loop diagram. Near $T \simeq T_c$, we can expand $V_{\text{eff}}(\phi_0)$ in ϕ_0/T and obtain

$$V_{\text{eff}}(\phi) - V_{\text{eff}}(0) \simeq \left[T \ln 2 - \frac{\mu}{\epsilon} \right] \left(\frac{m\phi_0}{2\pi} \right)^2 + \frac{\phi_0^2}{16T} \left(\frac{m\phi_0}{2\pi} \right)^2 + \dots \quad (42)$$

The second order phase transition occurs when the coefficient of the quadratic term in ϕ_0 vanishes. Accordingly, at $T = T_c$, the chemical potential is found to be

$$\mu = \epsilon T_c \ln 2 + O(\epsilon^2). \quad (43)$$

We then compute the $O(\epsilon)$ correction to the density $n = -\partial V_{\text{eff}}/\partial \mu$ in Eq. (40) at $T = T_c$ and hence $\phi_0 = 0$. For this purpose, we need to evaluate the fermion and boson one-loop diagrams with two μ insertions and the two-loop diagrams with one μ insertion to the fermion and boson propagators (Fig. 9). Performing the loop integrations and substituting Eq. (43), we can find

$$n = \left[\frac{3\pi^2}{2} - \left\{ \frac{3\pi^2 \ln 2 + 18\zeta'(2)}{4} + D - 2(\ln 2)^2 \right\} \epsilon \right] \left(\frac{mT_c}{2\pi} \right)^{d/2}, \quad (44)$$

where $D \approx 1.92181$ is a numerical constant. From the definition $\epsilon_F \equiv \frac{2\pi}{m} \left[\Gamma\left(\frac{d}{2} + 1\right) \frac{n}{2} \right]^{2/d}$, we obtain T_c/ϵ_F up to the next-leading order in ϵ :

$$\left. \frac{T_c}{\epsilon_F} \right|_{d \rightarrow 4} = 0.260 - 0.0112\epsilon + O(\epsilon^2). \quad (45)$$

On the other hand, because the unitary Fermi gas near $d = 2$ reduces to a weakly interacting Fermi gas, the critical temperature is provided by the usual BCS formula $T_c = (e^\gamma/\pi)\Delta$, where Δ is the energy gap of the fermion quasiparticle at zero temperature. Because Δ in the expansion over $\bar{\epsilon}$ is already obtained by $\bar{\phi}_0 = 2\mu e^{-1/\bar{\epsilon} - 1 + O(\bar{\epsilon})}$ in Eq. (23), we easily find

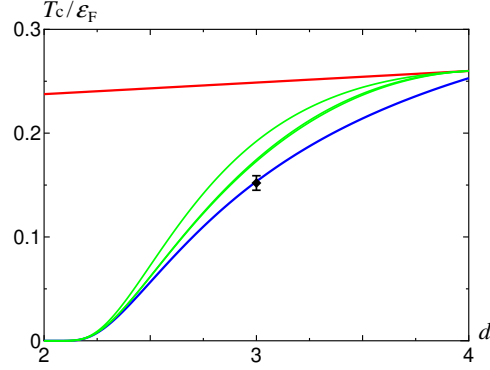


Fig. 10 Critical temperature T_c as a function of the spatial dimension d . The upper (lower) curve is the extrapolation from the NLO expansion around $d = 4$ in Eq. (45) [$d = 2$ in Eq. (46)]. The middle three curves show the Padé and Borel-Padé interpolations of the two NLO expansions. The symbol at $d = 3$ indicates the result $T_c/\epsilon_F = 0.152(7)$ from the Monte Carlo simulation [23].

$$\left. \frac{T_c}{\epsilon_F} \right|_{d \rightarrow 2} = \frac{2e^\gamma}{\pi} e^{-1/\bar{\epsilon} - 1 + O(\bar{\epsilon})}, \quad (46)$$

where we used $\mu/\epsilon_F = \xi = 1 + O(\epsilon)$ [Eq. (25)]. The exponential $e^{-1/\bar{\epsilon}}$ is equivalent to the mean field result while the correction e^{-1} corresponds to the Gor'kov-Melik-Barkhudarov correction in $d = 3$.

Now the value of T_c/ϵ_F in $d = 3$ can be extracted by interpolating the two expansions around $d = 4$ and $d = 2$ just as has been done for ξ in Sect. 2.3.1. We write T_c/ϵ_F in the form

$$\frac{T_c}{\epsilon_F} = \frac{2e^\gamma}{\pi} e^{-1/\bar{\epsilon} - 1} F(\bar{\epsilon}), \quad (47)$$

where $F(\bar{\epsilon})$ is an unknown function and the nonanalytic dependence on $\bar{\epsilon}$ was factored out. We approximate $F(\bar{\epsilon})$ or its Borel transform $G(t)$ by ratios of two polynomials and determine their coefficients so that T_c/ϵ_F in Eq. (47) has the correct NLO expansions both around $d = 4$ [Eq. (45)] and $d = 2$ [Eq. (46)]. Fig. 10 shows the behavior of T_c/ϵ_F as a function of d . The middle three curves are the Padé and Borel-Padé interpolations of the two NLO expansions. In $d = 3$, these interpolations give

$$\frac{T_c}{\epsilon_F} \approx 0.173, 0.175, 0.192, \quad (48)$$

which span an interval $T_c/\epsilon_F \approx 0.180 \pm 0.012$. Our interpolated values are not too far from the result of the Monte Carlo simulation $T_c/\epsilon_F = 0.152(7)$ [23]. For comparison, the mean field approximation yields $T_c/\epsilon_F \approx 0.496$.

2.6 Phase diagram of an imbalanced Fermi gas

The phase diagram of a density- and mass-imbalanced Fermi gas was studied using the ϵ expansion in Refs. [7, 19].

3 Aspects as a nonrelativistic conformal field theory

Because of the absence of scales in the zero-range and infinite scattering interaction, the theory describing fermions in the unitarity limit is a nonrelativistic conformal field theory (NRCFT). In this section, after deriving the Schrödinger algebra and the operator-state correspondence in NRCFTs, we compute the scaling dimensions of few-body composite operators exactly or with the help of the ϵ expansion, which provide the energies of a few fermions at unitarity in a harmonic potential.

3.1 Schrödinger algebra

We start with a brief review of the Schrödinger algebra [14, 15]. For the latter application, we allow spin- \uparrow and \downarrow fermions to have different masses m_\uparrow and m_\downarrow . We define the mass density:

$$\rho(\mathbf{x}) \equiv \sum_{\sigma=\uparrow,\downarrow} m_\sigma \psi_\sigma^\dagger(\mathbf{x}) \psi_\sigma(\mathbf{x}) \quad (49)$$

and the momentum density:

$$j_i(\mathbf{x}) \equiv -\frac{i}{2} \sum_{\sigma=\uparrow,\downarrow} [\psi_\sigma^\dagger(\mathbf{x}) \partial_i \psi_\sigma(\mathbf{x}) - \partial_i \psi_\sigma^\dagger(\mathbf{x}) \psi_\sigma(\mathbf{x})], \quad (50)$$

where $i = 1, \dots, d$ and the arguments of time are suppressed. The Schrödinger algebra is formed by the following set of operators:

Table 1 Part of the Schrödinger algebra. The values of $[X, Y]$ are shown below.

$X \setminus Y$	P_j	K_j	D	C	H
P_i	0	$-i\delta_{ij}M$	$-iP_i$	$-iK_i$	0
K_i	$i\delta_{ij}M$	0	iK_i	0	iP_i
D	iP_j	$-iK_j$	0	$-2iC$	$2iH$
C	iK_j	0	$2iC$	0	iD
H	0	$-iP_j$	$-2iH$	$-iD$	0

$$\text{mass : } M \equiv \int d\mathbf{x} \rho(\mathbf{x}) \quad (51)$$

$$\text{momentum : } P_i \equiv \int d\mathbf{x} j_i(\mathbf{x}) \quad (52)$$

$$\text{angular momentum : } J_{ij} \equiv \int d\mathbf{x} [x_i j_j(\mathbf{x}) - x_j j_i(\mathbf{x})] \quad (53)$$

$$\text{Galilean boost : } K_i \equiv \int d\mathbf{x} x_i \rho(\mathbf{x}) \quad (54)$$

$$\text{dilatation : } D \equiv \int d\mathbf{x} \mathbf{x} \cdot \mathbf{j}(\mathbf{x}) \quad (55)$$

$$\text{special conformal : } C \equiv \int d\mathbf{x} \frac{\mathbf{x}^2}{2} \rho(\mathbf{x}) \quad (56)$$

and the Hamiltonian:

$$H = \sum_{\sigma=\uparrow,\downarrow} \int d\mathbf{x} \frac{\partial \psi_{\sigma}^{\dagger}(\mathbf{x}) \cdot \partial \psi_{\sigma}(\mathbf{x})}{2m_{\sigma}} + \int d\mathbf{x} \int d\mathbf{y} \psi_{\uparrow}^{\dagger}(\mathbf{x}) \psi_{\downarrow}^{\dagger}(\mathbf{y}) V(|\mathbf{x} - \mathbf{y}|) \psi_{\downarrow}(\mathbf{y}) \psi_{\uparrow}(\mathbf{x}). \quad (57)$$

D and C are the generators of the scale transformation ($\mathbf{x} \rightarrow e^{\lambda} \mathbf{x}$, $t \rightarrow e^{2\lambda} t$) and the special conformal transformation [$\mathbf{x} \rightarrow \mathbf{x}/(1 + \lambda t)$, $t \rightarrow t/(1 + \lambda t)$], respectively. In a scale invariant system such as fermions in the unitarity limit, these operators form a closed algebra.⁵

Commutation relations of the above operators are summarized in Table 1. The rest of the algebra is the commutators of M , which commutes with all other operators; $[M, \text{any}] = 0$. The commutation relations of J_{ij} with other operators are determined by their transformation properties under rotations:

$$[J_{ij}, N] = [J_{ij}, D] = [J_{ij}, C] = [J_{ij}, H] = 0, \quad (58a)$$

$$[J_{ij}, P_k] = i(\delta_{ik} P_j - \delta_{jk} P_i), \quad [J_{ij}, K_k] = i(\delta_{ik} K_j - \delta_{jk} K_i), \quad (58b)$$

$$[J_{ij}, J_{kl}] = i(\delta_{ik} J_{jl} + \delta_{jl} J_{ik} - \delta_{il} J_{jk} - \delta_{jk} J_{il}). \quad (58c)$$

⁵ One potential that realizes the unitarity interaction is $V(r) = (\pi/2)^2 \lim_{r_0 \rightarrow 0} \theta(r_0 - r)/(2m_{\uparrow\downarrow} r_0^2)$, where $m_{\uparrow\downarrow} \equiv m_{\uparrow} m_{\downarrow}/(m_{\uparrow} + m_{\downarrow})$ is the reduced mass.

These commutation relations can be verified by direct calculations, while only the commutator of $[D, H] = 2iH$ requires the scale invariance of the Hamiltonian in which the interaction potential has to satisfy $V(e^\lambda r) = e^{-2\lambda}V(r)$.

3.2 Operator-state correspondence

3.2.1 Primary operators

We then introduce local operators $\mathcal{O}(t, \mathbf{x})$ as operators that depend on the position in time and space (t, \mathbf{x}) so that

$$\mathcal{O}(t, \mathbf{x}) = e^{iHt - iP_i x_i} \mathcal{O}(0) e^{-iHt + iP_i x_i}. \quad (59)$$

A local operator \mathcal{O} is said to have a scaling dimension $\Delta_{\mathcal{O}}$ and a mass $M_{\mathcal{O}}$ if it satisfies

$$[D, \mathcal{O}(0)] = i\Delta_{\mathcal{O}}\mathcal{O}(0) \quad \text{and} \quad [M, \mathcal{O}(0)] = M_{\mathcal{O}}\mathcal{O}(0). \quad (60)$$

With the use of the commutation relations in Table 1, we find that if a given local operator \mathcal{O} has the scaling dimension $\Delta_{\mathcal{O}}$, then the scaling dimensions of new local operators $[P_i, \mathcal{O}]$, $[H, \mathcal{O}]$, $[K_i, \mathcal{O}]$, and $[C, \mathcal{O}]$ are given by $\Delta_{\mathcal{O}} + 1$, $\Delta_{\mathcal{O}} + 2$, $\Delta_{\mathcal{O}} - 1$, and $\Delta_{\mathcal{O}} - 2$, respectively. Therefore, by repeatedly taking the commutators with K_i and C , one can keep to lower the scaling dimensions. However, this procedure has to terminate because the scaling dimensions of local operators are bounded from below as we will show in Sect. 3.2.3. The last operator \mathcal{O}_{pri} obtained in this way must have the property

$$[K_i, \mathcal{O}_{\text{pri}}(0)] = [C, \mathcal{O}_{\text{pri}}(0)] = 0. \quad (61)$$

Such operators that at $t = 0$ and $\mathbf{x} = \mathbf{0}$ commute with K_i and C will be called *primary operators*. Below the primary operator \mathcal{O}_{pri} is simply denoted by \mathcal{O} .

Starting with an arbitrary primary operator $\mathcal{O}(t, \mathbf{x})$, one can build up a tower of local operators by taking its commutators with P_i and H , in other words, by taking its space and time derivatives (left tower in Fig. 11). For example, the operators with the scaling dimension $\Delta_{\mathcal{O}} + 1$ in the tower are $[P_i, \mathcal{O}] = i\partial_i \mathcal{O}$. At the next level with the scaling dimension $\Delta_{\mathcal{O}} + 2$, the following operators are possible; $[P_i, [P_j, \mathcal{O}]] = -\partial_i \partial_j \mathcal{O}$ and $[H, \mathcal{O}] = -i\partial_t \mathcal{O}$. Commuting those operators with K_i and C , we can get back the operators into the lower rungs of the tower. The task of finding the spectrum of scaling dimensions of all local operators thus reduces to finding the scaling dimensions of all primary operators.

It is worthwhile to note that two-point correlation functions of the primary operators are constrained by the scale and Galilean invariance up to an overall constant [24]. For example, the two-point correlation function of the primary operator \mathcal{O} with its Hermitian conjugate is given by

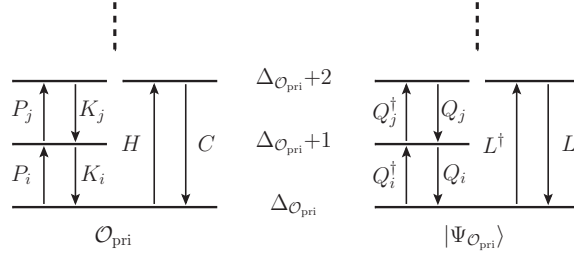


Fig. 11 Correspondence between the spectrum of scaling dimensions of local operators in NRCFT (left tower) and the energy spectrum of states in a harmonic potential (right tower). The bottom of each tower corresponds to the primary operator \mathcal{O}_{pri} (primary state $|\Psi_{\mathcal{O}_{\text{pri}}}\rangle$).

$$\langle T \mathcal{O}(t, \mathbf{x}) \mathcal{O}^\dagger(0) \rangle \propto \theta(t) t^{-\Delta_{\mathcal{O}}} \exp\left(i M_{\mathcal{O}^\dagger} \frac{|\mathbf{x}|^2}{2t}\right). \quad (62)$$

This formula or its Fourier transform $\propto \left(-p_0 + \frac{p^2}{2M_{\mathcal{O}^\dagger}} - i0^+\right)^{\Delta_{\mathcal{O}} - d/2 - 1}$ will be useful to read off the scaling dimension $\Delta_{\mathcal{O}}$.

3.2.2 Correspondence to states in a harmonic potential

We now show that each primary operator corresponds to an energy eigenstate of the system in a harmonic potential. The Hamiltonian of the system in a harmonic potential is

$$H_\omega \equiv H + \omega^2 C, \quad (63)$$

where ω is the oscillator frequency. We consider a primary operator $\mathcal{O}(t, \mathbf{x})$ that is composed of annihilation operators in the quantum field theory so that $\mathcal{O}^\dagger(t, \mathbf{x})$ acts nontrivially on the vacuum: $\mathcal{O}^\dagger|0\rangle \neq 0$. We construct the following state using \mathcal{O}^\dagger put at $t = 0$ and $\mathbf{x} = \mathbf{0}$:

$$|\Psi_{\mathcal{O}}\rangle \equiv e^{-H/\omega} \mathcal{O}^\dagger(0)|0\rangle. \quad (64)$$

If the mass of \mathcal{O}^\dagger is $M_{\mathcal{O}^\dagger} > 0$, then $|\Psi_{\mathcal{O}}\rangle$ is a mass eigenstate with the mass eigenvalue $M_{\mathcal{O}^\dagger}$: $M|\Psi_{\mathcal{O}}\rangle = M_{\mathcal{O}^\dagger}|\Psi_{\mathcal{O}}\rangle$. Furthermore, with the use of the commutation relations in Table 1, it is straightforward to show that $|\Psi_{\mathcal{O}}\rangle$ is actually an energy eigenstate of the Hamiltonian H_ω with the energy eigenvalue $E = \Delta_{\mathcal{O}}\omega$:

$$\begin{aligned} H_\omega |\Psi_{\mathcal{O}}\rangle &= (H + \omega^2 C) e^{-H/\omega} \mathcal{O}^\dagger(0)|0\rangle \\ &= e^{-H/\omega} (\omega^2 C - i\omega D) \mathcal{O}^\dagger(0)|0\rangle = \omega \Delta_{\mathcal{O}} |\Psi_{\mathcal{O}}\rangle, \end{aligned} \quad (65)$$

where we used $[C, \mathcal{O}^\dagger(0)] = 0$ and $[D, \mathcal{O}^\dagger(0)] = i\Delta_{\mathcal{O}}$ and the fact that both C and D annihilate the vacuum.

Table 2 Commutation relations of the Hamiltonian and the raising and lowering operators in the oscillator space. The values of $[X, Y]$ are shown below.

$X \setminus Y$	Q_j^\dagger	Q_j	H_ω/ω	L	L^\dagger
Q_i^\dagger	0	$-\delta_{ij}M$	$-Q_i^\dagger$	$-Q_i$	0
Q_i	$\delta_{ij}M$	0	Q_i	0	Q_i^\dagger
H_ω/ω	Q_j^\dagger	$-Q_j$	0	$-2L$	$2L^\dagger$
L	Q_j	0	$2L$	0	H_ω/ω
L^\dagger	0	$-Q_j^\dagger$	$-2L^\dagger$	$-H_\omega/\omega$	0

Starting with the primary state $|\Psi_{\mathcal{O}}\rangle$, one can build up a tower of energy eigenstates of H_ω by acting the following raising operators (right tower in Fig. 11):

$$Q_i^\dagger = \frac{P_i}{\sqrt{2\omega}} + i\sqrt{\frac{\omega}{2}}K_i \quad \text{and} \quad L^\dagger = \frac{H}{2\omega} - \frac{\omega}{2}C + \frac{i}{2}D. \quad (66)$$

From the commutation relations $[H_\omega, Q_i^\dagger] = \omega Q_i^\dagger$ and $[H_\omega, L^\dagger] = 2\omega L^\dagger$, Q_i^\dagger or L^\dagger acting on $|\Psi_{\mathcal{O}}\rangle$ raise its energy eigenvalue by ω or 2ω . For example, the states $(Q_i^\dagger)^n |\Psi_{\mathcal{O}}\rangle$ with $n = 0, 1, 2, \dots$ have their energy eigenvalues $E = (\Delta_{\mathcal{O}} + n)\omega$ and correspond to excitations of the center-of-mass motion in the i -direction, while $(L^\dagger)^n |\Psi_{\mathcal{O}}\rangle$ have $E = (\Delta_{\mathcal{O}} + 2n)\omega$ and correspond to excitations of the breathing mode [25]. The primary state $|\Psi_{\mathcal{O}}\rangle$ is annihilated by the lowering operators Q_i and L :

$$Q_i |\Psi_{\mathcal{O}}\rangle = 0 \quad \text{and} \quad L |\Psi_{\mathcal{O}}\rangle = 0. \quad (67)$$

Therefore $|\Psi_{\mathcal{O}}\rangle$ corresponds to the bottom of each semi-infinite tower of energy eigenstates, which is the ground state with respect to the center-of-mass and breathing mode excitations.

The commutation relations of the Hamiltonian and the raising and lowering operators in the oscillator space are summarized in Table 2. It is clear from the above arguments and also from Tables 1 and 2 that the roles of (P_i, K_i, D, C, H) in the free space is now played by $(Q_i^\dagger, Q_i, H_\omega, L, L^\dagger)$ in the oscillator space. Fig. 11 illustrates the correspondence between the spectrum of scaling dimensions of local operators in NRCFT and the energy spectrum of states in a harmonic potential.

The operator-state correspondence elucidated here allows us to translate the problem of finding the energy eigenvalues of the system in a harmonic potential to another problem of finding the scaling dimensions of primary operators in NRCFT. In Sect. 3.3, we use this correspondence to compute the energies of fermions at unitarity in a harmonic potential. We note that the similar correspondence between quantities in a harmonic potential and in a free space has been discussed in the quantum-mechanical language in Refs. [25, 26].

3.2.3 Unitarity bound of scaling dimensions

As we mentioned in Sect. 3.2.1, the scaling dimensions of local operators are bounded from below. The lower bound is equal to $d/2$, which can be seen from the following intuitive physical argument. According to the operator-state correspondence, the scaling dimension of a primary operator is the energy eigenvalue of particles in a harmonic potential. The latter can be divided into the center of mass energy and the energy of the relative motion. The ground state energy of the center of mass motion is $(d/2)\omega$, while the energy of the relative motion has to be non-negative [25]. Thus, energy eigenvalues, and hence operator dimensions, are bounded from below by $d/2$.

More formally, the lower bound can be derived from the requirement of non-negative norms of states in our theory [27]. We consider the primary state $|\Psi_{\mathcal{O}}\rangle$ whose mass and energy eigenvalues are given by $M_{\mathcal{O}^\dagger}$ and $\Delta_{\mathcal{O}}\omega$:

$$M|\Psi_{\mathcal{O}}\rangle = M_{\mathcal{O}^\dagger}|\Psi_{\mathcal{O}}\rangle \quad \text{and} \quad H_\omega|\Psi_{\mathcal{O}}\rangle = \Delta_{\mathcal{O}}\omega|\Psi_{\mathcal{O}}\rangle. \quad (68)$$

We then construct the following state:

$$|\Phi\rangle \equiv \left(L^\dagger - \sum_{i=1}^d \frac{Q_i^\dagger Q_i}{2M_{\mathcal{O}^\dagger}} \right) |\Psi_{\mathcal{O}}\rangle, \quad (69)$$

and require that it has a non-negative norm $\langle\Phi|\Phi\rangle \geq 0$. With the use of the commutation relations in Table 2 and Eq. (67), the norm of $|\Phi\rangle$ can be computed as

$$\langle\Phi|\Phi\rangle = \left(\Delta_{\mathcal{O}} - \frac{d}{2} \right) \langle\Psi_{\mathcal{O}}|\Psi_{\mathcal{O}}\rangle \geq 0. \quad (70)$$

Therefore we find the lower bound on the scaling dimensions of arbitrary primary operators:

$$\Delta_{\mathcal{O}} \geq \frac{d}{2}. \quad (71)$$

The lower bound $d/2$ multiplied by ω coincides with the ground state energy of a single particle in a d -dimensional harmonic potential.

When the primary state $|\Psi_{\mathcal{O}}\rangle$ saturates the lower bound $\Delta_{\mathcal{O}} = d/2$, the vanishing norm of $\langle\Phi|\Phi\rangle = 0$ means that the state itself is identically zero; $|\Phi\rangle \equiv 0$. Accordingly, the state created by the corresponding primary operator $\mathcal{O}(t, \mathbf{x})$ obeys the free Schrödinger equation:

$$\left[i\partial_t - \frac{\partial^2}{2M_{\mathcal{O}^\dagger}} \right] \mathcal{O}^\dagger(t, \mathbf{x})|0\rangle = 0. \quad (72)$$

In addition to the trivial one-body operator ψ_σ , we will see nontrivial examples of primary operators that saturate the lower bound of the scaling dimensions.

If a theory contains an operator \mathcal{O} with its scaling dimension between $d/2$ and $(d+2)/2$, then $\mathcal{O}^\dagger\mathcal{O}$ is a relevant deformation: $\Delta_{\mathcal{O}^\dagger\mathcal{O}} < d+2$. Therefore, such a

theory should contain a fine tuning in the $\mathcal{O}^\dagger \mathcal{O}$ channel. We will see this pattern explicitly below.

3.2.4 Nonuniversality of p -wave resonances

One consequence of the unitarity bound on operator dimensions is the impossibility of achieving universality in p -wave resonances in three spatial dimensions. This issue was raised in connection with the α - n scattering [28]. Theoretically, such a resonance would be described by the following Lagrangian density:

$$\mathcal{L} = \psi_\sigma^\dagger \left(i\partial_t + \frac{\partial^2}{2m} \right) \psi_\sigma + c_1 \phi_i^\dagger \left(i\partial_t + \frac{\partial^2}{4m} \right) \phi_i + c_2 \phi_i^\dagger \phi_i \quad (73)$$

$$+ (\psi_\uparrow^\dagger \partial_i \psi_\downarrow^\dagger - \partial_i \psi_\uparrow^\dagger \psi_\downarrow^\dagger) \phi_i + \phi_i^\dagger (\psi_\downarrow \partial_i \psi_\uparrow - \partial_i \psi_\downarrow \psi_\uparrow), \quad (74)$$

where c_1 and c_2 are bare couplings chosen to cancel out the divergences in the one-loop self-energy of ϕ_i . (In contrast to the s -wave resonance case, the loop integral is cubic divergent and requires two counter terms to regularize, corresponding to two simultaneous fine tunings of the scattering length and the effective range. In dimensional regularization, $c_1 = c_2 = 0$.) The field ϕ_i now has a finite propagator

$$\int dt d\mathbf{x} e^{ip_0 t - i\mathbf{p}\cdot\mathbf{x}} \langle T \phi_i(t, \mathbf{x}) \phi_i^\dagger(0) \rangle \propto \left(-p_0 + \frac{\mathbf{p}^2}{4m} - i0^+ \right)^{-d/2}. \quad (75)$$

Such a theory might appear healthy but the scaling dimension of ϕ_i , as one can see explicitly by comparing Eq. (75) with the Fourier transform of Eq. (62), is $\Delta_\phi = 1$ which is below the unitarity bound of $d/2$ in $d = 3$. (In a free theory $\Delta_\phi = d + 1$, but the fine tunings “reflect” Δ_ϕ with respect to $(d + 2)/2$ so that Δ_ϕ becomes 1.) Thus, p -wave resonances cannot be universal in three spatial dimensions. The proof given here is more general than that of Refs. [29]. Other examples considered in Refs. [29] can also be analyzed from the light of the unitarity bound.

3.3 Scaling dimensions of composite operators

All results derived in Sects. 3.1 and 3.2 can be applied to any NRCFTs. Here we concentrate on the specific system of spin- $\frac{1}{2}$ fermions in the unitarity limit and study various primary operators and their scaling dimensions. The simplest primary operator is the one-body operator $\psi_\sigma(\mathbf{x})$ whose scaling dimension is trivially given by

$$\Delta_{\psi_\sigma} = \frac{d}{2}. \quad (76)$$

This value multiplied by ω indeed matches the ground state energy of one fermion in a d -dimensional harmonic potential.

3.3.1 Two-body operator

The first nontrivial primary operator is the two-body composite operator: $\phi(\mathbf{x}) \equiv c_0 \psi_\downarrow \psi_\uparrow(\mathbf{x})$, which also appears as an auxiliary field of the Hubbard-Stratonovich transformation (8a). The presence of the prefactor $c_0 \sim \Lambda^{2-d}$ guarantees that matrix elements of $\phi(\mathbf{x})$ between two states in the Hilbert space are finite. Accordingly its scaling dimension becomes

$$\Delta_\phi = \Delta_{\psi_\uparrow} + \Delta_{\psi_\downarrow} + (2-d) = 2. \quad (77)$$

This result can be confirmed by computing the two-point correlation function of ϕ and comparing it with the Fourier transform of Eq. (62):

$$\int dt d\mathbf{x} e^{ip_0 t - i\mathbf{p}\cdot\mathbf{x}} \langle T \phi(t, \mathbf{x}) \phi^\dagger(0) \rangle = \frac{\left(\frac{2\pi}{m_{\uparrow\downarrow}}\right)^{d/2}}{\Gamma\left(1 - \frac{d}{2}\right) \left[-p_0 + \frac{\mathbf{p}^2}{2(m_\uparrow + m_\downarrow)} - i0^+\right]^{d/2-1}}. \quad (78)$$

According to the operator-state correspondence, the ground state energy of two fermions at unitarity in a harmonic potential is exactly 2ω for an arbitrary spatial dimension d . This result is consistent with our intuitive pictures of spin- \uparrow and \downarrow fermions in the unitarity limit as a single point-like composite boson in $d = 4$, two noninteracting fermions in $d = 2$, and two identical fermions in $d = 1$ (see discussions in Sects. 2.1.1 and 2.3.2). Note that $\phi(\mathbf{x})$ in $d = 4$ saturates the lower bound (71) and thus obeys the free Schrödinger equation (72) with mass $M_{\phi^\dagger} = m_\uparrow + m_\downarrow$. The same result in $d = 3$ has been obtained by directly solving the two-body Schrödinger equation with a harmonic potential [30], which is consistent with the experimental measurement [31].

3.3.2 Three-body operators

We then consider three-body composite operators. The formula to compute their scaling dimensions for arbitrary mass ratio m_\uparrow/m_\downarrow , angular momentum l , and spatial dimension d is derived in Appendix. Here we discuss its physical consequences in $d = 3$. Three-body operators composed of two spin- \uparrow and one spin- \downarrow fermions with orbital angular momentum $l = 0$ and $l = 1$ are

$$\mathcal{O}_{\uparrow\uparrow\downarrow}^{(l=0)}(\mathbf{x}) \equiv Z_0^{-1} \phi \psi_\uparrow(\mathbf{x}) \quad (79)$$

and

$$\mathcal{O}_{\uparrow\uparrow\downarrow}^{(l=1)}(\mathbf{x}) \equiv Z_1^{-1} [(m_\uparrow + m_\downarrow) \phi \partial_i \psi_\uparrow - m_\uparrow (\partial_i \phi) \psi_\uparrow](\mathbf{x}), \quad (80)$$

where $i = 1, 2, 3$ and $Z_l \sim \Lambda^{-\mathcal{N}}$ is the renormalization factor. The mass factors in Eq. (80) are necessary so that the operator is primary; $[K_i, \mathcal{O}_{\uparrow\uparrow\downarrow}^{(l=1)}(0)] = 0$.

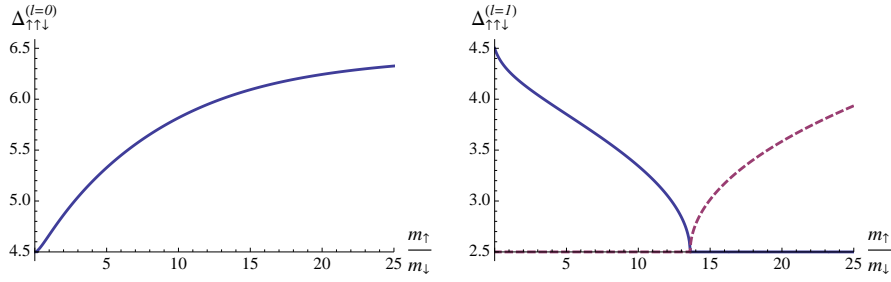


Fig. 12 Scaling dimensions of three-body composite operators $\mathcal{O}_{\uparrow\uparrow\downarrow}^{(l)}$ with angular momentum $l = 0$ (left panel) and $l = 1$ (right panel) as functions of the mass ratio $m_{\uparrow}/m_{\downarrow}$. In the right panel, the real part (solid curve) and the imaginary part shifted by $+2.5$ (dashed curve) are plotted.

Their scaling dimensions $\Delta_{\uparrow\uparrow\downarrow}^{(l)} = \frac{7}{2} + l + \gamma_l$ obtained by solving Eq. (135) are plotted in Fig. 12 as functions of the mass ratio $m_{\uparrow}/m_{\downarrow}$. For $l = 0$ (left panel), $\Delta_{\uparrow\uparrow\downarrow}^{(l)}$ increases as $m_{\uparrow}/m_{\downarrow}$ is increased indicating the stronger effective repulsion in the s -wave channel. On the other hand, $\Delta_{\uparrow\uparrow\downarrow}^{(l)}$ for $l = 1$ (right panel) decreases with increasing $m_{\uparrow}/m_{\downarrow}$ and eventually, when the mass ratio exceeds the critical value $m_{\uparrow}/m_{\downarrow} > 13.607$, it becomes complex as $\Delta_{\uparrow\uparrow\downarrow}^{(l=1)} = \frac{5}{2} \pm i\text{Im}(\gamma_1)$.⁶ In this case, the Fourier transform of Eq. (62) implies that the two-point correlation function of $\mathcal{O}_{\uparrow\uparrow\downarrow}^{(l=1)}$ behaves as

$$\propto \sin \left[\text{Im}(\gamma_1) \ln \left(\frac{\mathbf{p}^2 - (4m_{\uparrow} + 2m_{\downarrow})p_0 - i0^+}{\Lambda^2} \right) + \theta \right]. \quad (81)$$

Now the full scale invariance of the original NRCFT is broken down to a discrete scaling symmetry,

$$\mathbf{p} \rightarrow e^{n\pi/\text{Im}(\gamma_1)} \mathbf{p} \quad \text{and} \quad p_0 \rightarrow e^{2n\pi/\text{Im}(\gamma_1)} p_0, \quad (82)$$

with n being an integer. This is a characteristic of the renormalization-group limit cycle and related to the existence of an infinite set of three-body bound states in the p -wave channel. Their energy eigenvalues form a geometric spectrum $E_{n+1}/E_n = e^{-2\pi/|\text{Im}(\gamma_1)|}$, which is known as the Efimov effect [32]. Because the system develops deep three-body bound states, the corresponding many-body system cannot be stable toward collapse.

We note that, in the range of the mass ratio $8.6186 < m_{\uparrow}/m_{\downarrow} < 13.607$, the scaling dimension of $\mathcal{O}_{\uparrow\uparrow\downarrow}^{(l=1)}$ satisfies $\frac{5}{2} < \Delta_{\uparrow\uparrow\downarrow}^{(l=1)} < \frac{7}{2}$. Accordingly the following three-body interaction term

$$\mathcal{L}_{3\text{-body}} = c_1 \mathcal{O}_{\uparrow\uparrow\downarrow}^{(1)\dagger}(t, \mathbf{x}) \mathcal{O}_{\uparrow\uparrow\downarrow}^{(1)}(t, \mathbf{x}) \quad (83)$$

⁶ This situation illustrates a general feature: onsets of the Efimov effect occur when the ground state energy of the corresponding few-body system in a harmonic potential is equal to $\frac{d+2}{2}\omega$.

becomes renormalizable because now the coupling has the dimension $-2 < [c_1] < 0$. The Lagrangian density (8a) with $\mathcal{L}_{3\text{-body}}$ added defines a new renormalizable theory. In particular, when the coupling c_1 is tuned to its nontrivial fixed point ($c_1 \neq 0$) that describes a three-body resonance in the p -wave channel, the resulting theory provides a novel NRCFT. The corresponding system is that of spin- $\frac{1}{2}$ fermions with both two-body ($\uparrow\downarrow$) and three-body ($\uparrow\uparrow\downarrow$) resonances and its many-body physics was studied in Ref. [16].

3.4 Application of the ϵ expansion

It would be difficult to determine exact scaling dimensions of composite operators with more than three fermions in $d = 3$. However, it is possible to estimate them with the help of the ϵ expansions around $d = 4$ and $d = 2$. The formulations developed in Sect. 2.2 can be used for the few-body problems as well just by setting $\mu = \phi_0 = 0$. Here we concentrate on the equal mass case $m_\uparrow = m_\downarrow$.

3.4.1 Scaling dimensions near four spatial dimensions

The scaling dimensions of composite operators can be determined by studying their renormalizations. We start with the simplest three-body operator $\phi\psi_\uparrow$ near $d = 4$, which has zero orbital angular momentum $l = 0$. The leading-order diagram that renormalizes $\phi\psi_\uparrow$ is $O(\epsilon)$ and depicted in Fig. 13 (left). Performing the loop integration, we find that this diagram is logarithmically divergent at $d = 4$ and thus the renormalized operator differs from the bare one by the renormalization factor; $(\phi\psi_\uparrow)_{\text{ren}} = Z_{\phi\psi_\uparrow}^{-1} \phi\psi_\uparrow$, where $Z_{\phi\psi_\uparrow} = 1 - \frac{4}{3}\epsilon \ln\Lambda$. From the anomalous dimension $\gamma_{\phi\psi_\uparrow} = -\ln Z_{\phi\psi_\uparrow} / \ln\Lambda = \frac{4}{3}\epsilon$, we obtain the scaling dimension of the renormalized operator up to the next-to-leading order in ϵ :

$$\Delta_{\phi\psi_\uparrow} = \Delta_\phi + \Delta_{\psi_\uparrow} + \gamma_{\phi\psi_\uparrow} = 4 + \frac{5}{6}\epsilon + O(\epsilon^2). \quad (84)$$

According to the operator-state correspondence, there is a three-fermion state in a harmonic potential with $l = 0$ and energy equal to $E_3^{(0)} = \Delta_{\phi\psi_\uparrow} \omega$, which continues to the first excited state in $d = 3$. Even within the leading correction in ϵ , the naive extrapolation to $\epsilon \rightarrow 1$ yields $E_3^{(0)} \rightarrow 4.83 \omega$, which is already close to the true first excited state energy 4.66622ω in $d = 3$ [26].

The ground state of three fermions in a harmonic potential has $l = 1$ in $d = 3$. The corresponding primary operator near $d = 4$ is $2\phi\partial\psi_\uparrow - (\partial\phi)\psi_\uparrow$, which is renormalized by the same diagram in Fig. 13 (left). From its anomalous dimension $\gamma = -\ln Z / \ln\Lambda = -\frac{1}{3}\epsilon$, we obtain the scaling dimension of the renormalized operator up to the next-to-leading order in ϵ :

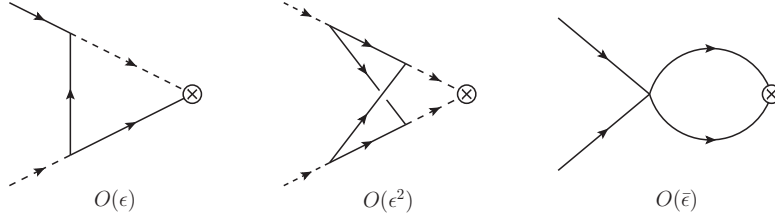


Fig. 13 Leading-order Feynman diagrams to renormalize the composite operators $\phi\psi_{\uparrow}$ (left) and $\phi\phi$ (middle) near $d = 4$ and $\psi_{\uparrow}\psi_{\downarrow}$ (right) near $d = 2$. These operators are inserted at \otimes .

$$\Delta_{2\phi\partial\psi_{\uparrow}-(\partial\phi)\psi_{\uparrow}} = \Delta_{\phi} + \Delta_{\psi_{\uparrow}} + 1 + \gamma = 5 - \frac{5}{6}\epsilon + O(\epsilon^2). \quad (85)$$

The operator-state correspondence tells us that the three-fermion state in a harmonic potential with $l = 1$ has the energy $E_3^{(1)} = \Delta_{2\phi\partial\psi_{\uparrow}-(\partial\phi)\psi_{\uparrow}}\omega$. The naive extrapolation to $\epsilon \rightarrow 1$ yields $E_3^{(1)} \rightarrow 4.17\omega$, which is already close to the true ground state energy 4.27272ω in $d = 3$ [26].

We now turn to the lowest four-body operator $\phi\phi$ with zero orbital angular momentum $l = 0$. The first nontrivial correction to its scaling dimension is $O(\epsilon^2)$ given by the diagram depicted in Fig. 13 (middle). The two-loop integral can be done analytically and we obtain the renormalization factor; $Z_{\phi\phi} = 1 - 8\epsilon^2 \ln \frac{27}{16} \ln \Lambda$. Therefore we find the scaling dimension of the renormalized operator $(\phi\phi)_{\text{ren}} = Z_{\phi\phi}^{-1}\phi\phi$ to be

$$\Delta_{\phi\phi} = 2\Delta_{\phi} + \gamma_{\phi\phi} = 4 + 8\epsilon^2 \ln \frac{27}{16} + O(\epsilon^3). \quad (86)$$

According to the operator-state correspondence, the ground state of four fermions in a harmonic potential has the energy $E_4^{(0)} = \Delta_{\phi\phi}\omega$. Because the $O(\epsilon^2)$ correction turns out to be large, we shall not directly extrapolate Eq. (86) to $\epsilon \rightarrow 1$ but will combine it with an expansion near $d = 2$.

The above results can be easily extended to a general number of fermions by evaluating the diagrams in Fig. 13 with more boson lines attached. The primary operators having N fermion number and orbital angular momentum l are summarized in Table 3 with their scaling dimensions computed in the ϵ expansion. The energy of the corresponding state in a harmonic potential is simply given by $E_N^{(l)} = \Delta_{\mathcal{O}}\omega$. The leading-order results [$E_N^{(0)} = N\omega$ for even N and $E_N^{(0)} = (N+1)\omega$ and $E_N^{(1)} = (N+2)\omega$ for odd N] can be intuitively understood by recalling that fermion pairs at unitarity in $d = 4$ form point-like bosons and they do not interact with each other or with extra fermions. Therefore the ground state of $N = 2n$ fermions consists of n free composite bosons occupying the same lowest energy state in a harmonic potential with the energy 2ω in $d = 4$. When $N = 2n + 1$, the ground state has $l = 0$ and consists of n composite bosons and one extra fermion occupying the same lowest energy state again. In order to create an $l = 1$ state, one

Table 3 N -body composite operators with angular momentum l near $d = 4$ and their scaling dimensions in the ϵ expansion.

N (l)	$\mathcal{O}_N^{(l)}$	$\Delta_{\mathcal{O}}$
$2n$ ($l = 0$)	ϕ^n	$N + N(N-2)\epsilon^2 \ln \frac{27}{16} + \mathcal{O}(\epsilon^3)$
$2n+1$ ($l = 0$)	$\phi^n \phi_{\uparrow}$	$N + 1 + \frac{4N-7}{6}\epsilon + \mathcal{O}(\epsilon^2)$
$2n+1$ ($l = 1$)	$2\phi^n \partial \psi_{\uparrow} - \phi^{n-1}(\partial \phi) \psi_{\uparrow}$	$N + 2 + \frac{2N-21}{18}\epsilon + \mathcal{O}(\epsilon^2)$

of the $n+1$ particles has to be excited to the first excited state, which costs the additional energy 1ω . The leading correction to the energy, which is represented by the anomalous dimension in NRCFT, originates from the weak boson-fermion [$\mathcal{O}(\epsilon)$] or boson-boson [$\mathcal{O}(\epsilon^2)$] interaction. Finally we note that in $d = 4$, we can observe the odd-even staggering in the ground state energy; $E_N^{(0)} - (E_{N-1}^{(0)} + E_{N+1}^{(0)})/2 = 1\omega$ for odd N .

3.4.2 Scaling dimensions near two spatial dimensions

Similarly, we can determine the scaling dimensions of composite operators near $d = 2$ by studying their renormalizations. Here we consider the three-body operators $\psi_{\uparrow}\psi_{\downarrow}\partial_t\psi_{\uparrow}$ and $\psi_{\uparrow}\psi_{\downarrow}\partial\psi_{\uparrow}$, which are primary and have the orbital angular momentum $l = 0$ and $l = 1$, respectively. The leading-order diagrams that renormalize them are $\mathcal{O}(\bar{\epsilon})$ and depicted in Fig. 13 (right) with one more fermion line attached. Performing the loop integrations, we find that these diagrams are logarithmically divergent at $d = 2$ and thus the renormalized operators differ from the bare ones by the renormalization factors; $Z_{\psi_{\uparrow}\psi_{\downarrow}\partial_t\psi_{\uparrow}} = 1 + \frac{3}{2}\bar{\epsilon}\ln\Lambda$ and $Z_{\psi_{\uparrow}\psi_{\downarrow}\partial\psi_{\uparrow}} = 1 + \frac{3}{2}\bar{\epsilon}\ln\Lambda$. From the anomalous dimensions $\gamma_{\mathcal{O}} = -\ln Z_{\mathcal{O}}/\ln\Lambda = -\frac{3}{2}\bar{\epsilon}$, we obtain the scaling dimensions of the renormalized operators up to the next-to-leading order in $\bar{\epsilon}$:

$$\Delta_{\psi_{\uparrow}\psi_{\downarrow}\partial_t\psi_{\uparrow}} = 3\Delta_{\psi_{\sigma}} + 2 + \gamma_{\psi_{\uparrow}\psi_{\downarrow}\partial_t\psi_{\uparrow}} = 5 + \mathcal{O}(\bar{\epsilon}^2) \quad (87)$$

and

$$\Delta_{\psi_{\uparrow}\psi_{\downarrow}\partial\psi_{\uparrow}} = 3\Delta_{\psi_{\sigma}} + 1 + \gamma_{\psi_{\uparrow}\psi_{\downarrow}\partial\psi_{\uparrow}} = 4 + \mathcal{O}(\bar{\epsilon}^2). \quad (88)$$

The operator-state correspondence tells us that the three-fermion states in a harmonic potential with $l = 0$ and $l = 1$ have the energies $E_3^{(0)} = \Delta_{\psi_{\uparrow}\psi_{\downarrow}\partial_t\psi_{\uparrow}}\omega$ and $E_3^{(1)} = \Delta_{\psi_{\uparrow}\psi_{\downarrow}\partial\psi_{\uparrow}}\omega$, respectively.

We can develop the same analysis for composite operators with more than three fermions by evaluating the diagram in Fig. 13 (right) with more fermion lines attached. The primary operators having $N \leq 6$ fermion number and orbital angular momentum l are summarized in Table 4 with their scaling dimensions computed in the $\bar{\epsilon}$ expansion. Note that composite operators having the same classical dimen-

Table 4 N -body composite operators with angular momentum l near $d = 2$ and their scaling dimensions in the $\bar{\epsilon}$ expansion. Known values for the energies of N fermions in a harmonic potential in $d = 3$ are also shown in units of $\hbar\omega$.

N (l)	$\mathcal{O}_N^{(l)}$	$\Delta_{\mathcal{O}}$	$E/\hbar\omega$ in $d = 3$
2 ($l = 0$)	$\psi_{\uparrow}\psi_{\downarrow}$	2	2 [30]
3 ($l = 0$)	$\psi_{\uparrow}\psi_{\downarrow}(\partial_t\psi_{\uparrow})$	$5 + O(\bar{\epsilon}^2)$	4.66622 [26]
3 ($l = 1$)	$\psi_{\uparrow}\psi_{\downarrow}(\partial\psi_{\uparrow})$	$4 + O(\bar{\epsilon}^2)$	4.27272 [26]
4 ($l = 0$)	$\psi_{\uparrow}\psi_{\downarrow}(\partial\psi_{\uparrow}\cdot\partial\psi_{\downarrow})$	$6 - \bar{\epsilon} + (\bar{\epsilon}^2)$	≈ 5.028 [33]
5 ($l = 0$)	(*)	$9 - \frac{11 \pm \sqrt{105}}{16}\bar{\epsilon} + O(\bar{\epsilon}^2)$	≈ 8.03 [33]
5 ($l = 1$)	$\psi_{\uparrow}\psi_{\downarrow}(\partial\psi_{\uparrow}\cdot\partial\psi_{\downarrow})\partial\psi_{\uparrow}$	$8 - \bar{\epsilon} + O(\bar{\epsilon}^2)$	≈ 7.53 [33]
6 ($l = 0$)	$\psi_{\uparrow}\psi_{\downarrow}(\partial\psi_{\uparrow}\cdot\partial\psi_{\downarrow})^2$	$10 - 2\bar{\epsilon} + (\bar{\epsilon}^2)$	≈ 8.48 [33]

$$(*) = a\psi_{\uparrow}\psi_{\downarrow}(\partial\psi_{\uparrow}\cdot\partial\psi_{\downarrow})\partial^2\psi_{\uparrow} + b\psi_{\uparrow}\partial_t\psi_{\downarrow}(\partial\psi_{\uparrow}\cdot\partial\psi_{\downarrow})\partial_t\psi_{\uparrow} + c\psi_{\uparrow}\psi_{\downarrow}((\partial_t\partial\psi_{\uparrow})\cdot\partial\psi_{\downarrow})\partial_t\psi_{\uparrow} - d\psi_{\uparrow}\psi_{\downarrow}(\partial\psi_{\uparrow}\cdot\partial\psi_{\downarrow})i\partial_t\psi_{\uparrow} \text{ with } (a, b, c, d) = (\pm 19\sqrt{3} - 5\sqrt{35}, \mp 16\sqrt{3}, -6\sqrt{35} \mp 6\sqrt{3}, 16\sqrt{35}).$$

sion can mix under the renormalization and thus the primary operator with the well-defined scaling dimension may have a complicated form such as for $N = 5$ and $l = 0$. The leading order results for the corresponding energies $E_N^{(l)} = \Delta_{\mathcal{O}}\omega$ in a harmonic potential can be easily understood by recalling that fermions at unitarity become noninteracting in $d = 2$. Therefore the energy eigenvalue of each N -fermion state is just a sum of single particle energies in a harmonic potential in $d = 2$, and obviously, the ground state energy shows the shell structure. The $O(\bar{\epsilon})$ correction to the energy, which is represented by the anomalous dimension in NRCFT, originates from the weak fermion-fermion interaction. We can see in Table 4 the rough agreement of the naive extrapolations of $\Delta_{\mathcal{O}}$ to $\bar{\epsilon} \rightarrow 1$ with the known values in $d = 3$.

3.4.3 Interpolations of ϵ expansions

We now extract the energy of N fermions in a harmonic potential in $d = 3$ by interpolating the two expansions around $d = 4$ and $d = 2$ just as has been done for ξ in Sect. 2.3 and T_c/ϵ_F in Sect. 2.5. We approximate $E_N^{(l)}/\omega$ by ratios of two polynomials (Padé approximants) and determine their unknown coefficients so that the correct expansions both around $d = 4$ (Table 3) and $d = 2$ (Table 4) are reproduced.

Fig. 14 shows the behaviors of the three-fermion energies $E_{N=3}^{(l)}$ with orbital angular momentum $l = 0$ (left panel) and $l = 1$ (right panel) as functions of d . The middle four curves are the Padé interpolations of the two NLO expansions. Because the exact results for arbitrary d can be obtained from Eqs. (135) and (136), we can use this case as a benchmark test of our interpolation scheme. We find that the behaviors of the interpolated curves are quite consistent with the exact results even within the leading corrections in ϵ and $\bar{\epsilon}$. In $d = 3$, these interpolations give

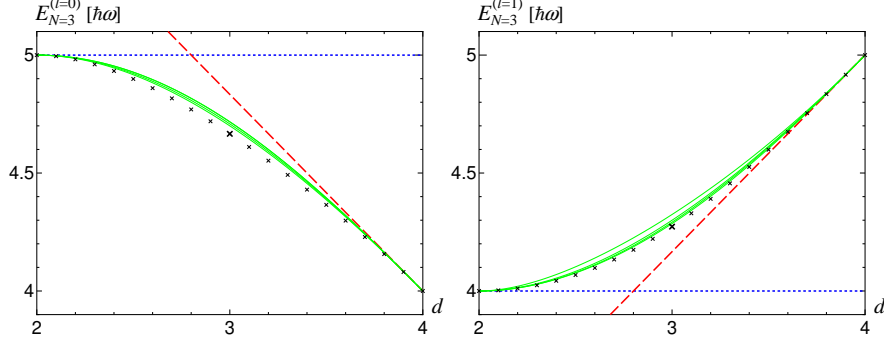


Fig. 14 Energies of three fermions in a harmonic potential in the s -wave channel $l = 0$ (left panel) and in the p -wave channel $l = 1$ (right panel) as functions of the spatial dimension d . The dashed (dotted) lines are the extrapolations from the NLO expansions around $d = 4$ in Eqs. (84) and (85) [$d = 2$ in Eqs. (87) and (88)]. The four solid curves show the Padé interpolations of the two NLO expansions. The symbols (\times) indicate the exact values for each d obtained from Eqs. (135) and (136).

$$\frac{E_{N=3}^{(l=0)}}{\omega} \approx 4.71, 4.7, 4.72, 4.72 \quad (89)$$

and

$$\frac{E_{N=3}^{(l=1)}}{\omega} \approx 4.29, 4.3, 4.32, 4.29, \quad (90)$$

which span very small intervals $E_3^{(0)}/\omega \approx 4.71 \pm 0.01$ and $E_3^{(1)}/\omega \approx 4.30 \pm 0.02$. Our interpolated values are reasonably close to the exact results 4.66622ω and 4.27272ω in $d = 3$ [26].

Here we comment on the convergence of the ϵ expansions around $d = 4$ and $d = 2$. By performing the expansions up to $O(\epsilon^{50})$ with the use of the exact formula in Eq. (135) and studying their asymptotic behaviors, we can find that the ϵ expansions are convergent at least for these three-body problems. Their radii of convergence are estimated to be $|\epsilon| \lesssim 0.48$ and $|\bar{\epsilon}| \lesssim 1.0$ for the $l = 0$ case and $|\epsilon| \lesssim 1.4$ and $|\bar{\epsilon}| \lesssim 1.0$ for the $l = 1$ case.

The same analysis can be done for the energies of more than three fermions in a harmonic potential where exact results are not available. The Padé interpolations of the two NLO expansions for $N = 5$ yield

$$\frac{E_{N=5}^{(l=0)}}{\omega} \approx 7.71, 7.64, 7.66, 7.82 \quad (91)$$

and

$$\frac{E_{N=5}^{(l=1)}}{\omega} \approx 7.10, 7.16, 7.19, 7.09 \quad (92)$$

in $d = 3$, which span relatively small intervals $E_5^{(0)}/\omega \approx 7.73 \pm 0.09$ and $E_5^{(1)}/\omega \approx 7.14 \pm 0.05$. On the other hand, the Padé interpolations of the two NLO expansions for $N = 4, 6$ yield

$$\frac{E_{N=4}^{(l=0)}}{\omega} \approx 5.55, 4.94, 4.94, 4.90, 6.17 \quad (93)$$

and

$$\frac{E_{N=6}^{(l=0)}}{\omega} \approx 10.1, 7.92, 7.92, 7.80, 16.4 \quad (94)$$

in $d = 3$. The first and last values corresponding to the Padé approximants where all terms are distributed to the numerator or denominator are considerably off from the other three values. This would be because of the large NLO corrections near $d = 4$. If such two extreme cases are excluded, the other three values span rather small intervals $E_4^{(0)}/\omega \approx 4.92 \pm 0.02$ and $E_6^{(0)}/\omega \approx 7.86 \pm 0.06$. For comparison, the numerical results obtained by using a basis set expansion technique are shown in Table 4 [33].

4 General coordinate and conformal invariance

Some nontrivial results can be obtained for the unitary Fermi gas using general symmetry arguments. For this end it is convenient to couple the unitary Fermi gas to an external gauge field A_μ ($\mu = 0, 1, 2, 3$) and to an external metric g_{ij} . Both A_μ and g_{ij} can be functions of time and space. Now the action of the unitary Fermi gas becomes

$$S = \int dt d\mathbf{x} \sqrt{g} \left(\frac{i}{2} \psi_\sigma^\dagger D_t \psi_\sigma - \frac{i}{2} D_t \psi_\sigma^\dagger \psi_\sigma - \frac{1}{2m} g^{ij} D_i \psi_\sigma^\dagger D_j \psi_\sigma + \psi_\uparrow^\dagger \psi_\downarrow^\dagger \phi + \phi^\dagger \psi_\downarrow \psi_\uparrow \right), \quad (95)$$

where $D_t = \partial_t - iA_0$ and $D_i = \partial_i - iA_i$ are covariant derivatives. We can see that A_0 plays the role of the external trapping potential. Recall that when the dimensional regularization is used, the term $\propto \phi^\dagger \phi$ is absent in the unitarity limit.

By direct calculations, one can verify that this action is invariant under the following transformations:

- Gauge transforms

$$\psi \rightarrow e^{i\alpha(t, \mathbf{x})} \psi, \quad \phi \rightarrow e^{2i\alpha(t, \mathbf{x})} \phi \quad (96a)$$

$$A_0 \rightarrow A_0 - \partial_t \alpha, \quad A_i \rightarrow A_i - \partial_i \alpha \quad (96b)$$

- General coordinate transformations

$$x^i \rightarrow x'^i, \quad x^i = x^i(t, x'^i) \quad (97a)$$

$$\psi(t, \mathbf{x}) \rightarrow \psi'(t, \mathbf{x}') = \psi(t, \mathbf{x}) \quad (97b)$$

$$\phi(t, \mathbf{x}) \rightarrow \phi'(t, \mathbf{x}') = \phi(t, \mathbf{x}) \quad (97c)$$

$$g_{ij}(t, \mathbf{x}) \rightarrow g'_{ij}(t, \mathbf{x}') = \frac{\partial x^i}{\partial x'^i} \frac{\partial x^j}{\partial x'^j} g_{ij}(t, \mathbf{x}) \quad (97d)$$

$$A_0(t, \mathbf{x}) \rightarrow A_0'(t, \mathbf{x}') = A_0(t, \mathbf{x}) + \dot{x}^i A_i - \frac{1}{2} \dot{x}^i \dot{x}^j g_{ij} \quad (97e)$$

$$A_i(t, \mathbf{x}) \rightarrow A_i'(t, \mathbf{x}') = \frac{\partial x^i}{\partial x'^i} A_i(t, \mathbf{x}) - \frac{\partial x^i}{\partial x'^i} \dot{x}^j g_{ij}(t, \mathbf{x}) \quad (97f)$$

- Conformal transformations

$$t \rightarrow t', \quad t = t(t') \quad (98a)$$

$$\psi(t, \mathbf{x}) \rightarrow \psi'(t', \mathbf{x}) = \left(\frac{\partial t}{\partial t'} \right)^{3/4} \psi(t, \mathbf{x}) \quad (98b)$$

$$\phi(t, \mathbf{x}) \rightarrow \phi'(t', \mathbf{x}) = \left(\frac{\partial t}{\partial t'} \right) \phi(t, \mathbf{x}) \quad (98c)$$

$$A_0(t, \mathbf{x}) \rightarrow A_0'(t', \mathbf{x}) = \left(\frac{\partial t}{\partial t'} \right) A_0(t, \mathbf{x}) \quad (98d)$$

$$A_i(t, \mathbf{x}) \rightarrow A_i'(t', \mathbf{x}) = A_i(t, \mathbf{x}) \quad (98e)$$

$$g_{ij}(t, \mathbf{x}) \rightarrow g'_{ij}(t', \mathbf{x}) = \left(\frac{\partial t}{\partial t'} \right)^{-1} g_{ij}(t, \mathbf{x}). \quad (98f)$$

These symmetries allow one to transform the unitary Fermi gas in a free space into that in a harmonic potential with an arbitrary time-dependent frequency $\omega(t)$. This is done by a combination of a conformal transformation $t = f(t')$, a general coordinate transformation

$$x^i = \lambda^{-1}(t) x'^i \quad \text{with} \quad \lambda(t) = [f'(t)]^{-1/2}, \quad (99)$$

and a gauge transformation with

$$\alpha = \frac{1}{2} \frac{\dot{\lambda}}{\lambda} x^2. \quad (100)$$

If one starts with $A_\mu = 0$ and $g_{ij} = \delta_{ij}$, these three transformations leave the gauge vector potential A_i and the metric g_{ij} unchanged, but generate a scalar potential A_0 :

$$A_0 = \frac{1}{2} \omega^2(t) x^2 \quad \text{with} \quad \omega^2(t) = -\frac{1}{2} \frac{\ddot{\lambda}}{\lambda}. \quad (101)$$

The transformed field operator is

$$\psi'(t, \mathbf{x}) = \exp\left(\frac{i}{2} \frac{\dot{\lambda}}{\lambda} x^2\right) \lambda^{-3/2}(t) \psi(f(t), \lambda^{-1}(t) \mathbf{x}). \quad (102)$$

This map between the unitary Fermi gas in the free space and that in the harmonic potential with the time-dependent frequency was previously found in Ref. [34].

In future applications, we only need the infinitesimal forms of the transformations. For reference, they are

$$\delta\psi = i\alpha\psi - \xi^k \partial_k \psi, \quad (103a)$$

$$\delta A_0 = -\dot{\alpha} - \xi^k \partial_k A_0 - A_k \dot{\xi}^k, \quad (103b)$$

$$\delta A_i = -\partial_i \alpha - \xi^k \partial_k A_i - A_k \partial_i \xi^k + m g_{ik} \dot{\xi}^k, \quad (103c)$$

$$\delta g_{ij} = -\xi^k \partial_k g_{ij} - g_{ik} \partial_j \xi^k - g_{kj} \partial_i \xi^k \quad (103d)$$

for the gauge and general coordinate transformations, and

$$\delta O = -\beta \dot{O} - \frac{1}{2} \Delta[O] \dot{\beta} O \quad (104)$$

for the conformal transformations, where $\Delta[O]$ is the dimension of a field O ; $\Delta[\psi] = \frac{3}{2}$, $\Delta[\phi] = 2$, $\Delta[A_0] = 2$, $\Delta[A_i] = 0$, and $\delta[g_{ij}] = -2$.

4.1 Vanishing bulk viscosities

One consequence of the general coordinate and conformal invariance is the vanishing of the bulk viscosity of the unitarity Fermi gas in the normal phase, and the vanishing of two (out of three) bulk viscosities in the superfluid phase. These conclusions come from the requirement that hydrodynamic equations describing the motion of a fluid in the external gauge field and metric possess the same set of symmetries as the microscopic theory.

4.1.1 Normal phase

In the normal phase, the hydrodynamic equations are written in term of the local mass density ρ , the local velocity v^i , and the local entropy per unit mass s . These equations are

$$\frac{1}{\sqrt{g}} \partial_t (\sqrt{g} \rho) + \nabla_i (\rho v^i) = 0, \quad (105)$$

$$\frac{1}{\sqrt{g}} \partial_t (\sqrt{g} \rho v_i) + \nabla_k \Pi_i^k = \frac{\rho}{m} (E_i - F_{ik} v^k), \quad (106)$$

$$\frac{1}{\sqrt{g}} \partial_t (\sqrt{g} \rho s) + \nabla_i \left(\rho v^i \partial_i s - \frac{\kappa}{T} \partial^i T \right) = \frac{2R}{T}, \quad (107)$$

where Π_{ik} is the stress tensor, κ is the thermal conductivity, and R is the dissipative function. Compared to the usual equations written for the flat metric and in the absence of the gauge field, we have replaced the derivatives ∂_i by the covariant derivatives ∇_i and added the force term in the momentum conservation equation (106), which comes from the electric force ($E_i = \partial_t A_i - \partial_i A_0$) and the magnetic Lorentz force ($F_{ik} = \partial_i A_k - \partial_k A_i$). The stress tensor can be written as

$$\Pi_{ik} = \rho v_i v_k + p g_{ik} - \sigma'_{ik}, \quad (108)$$

where p is the pressure and σ'_{ik} is the viscous stress tensor. The information about the kinetic coefficients is contained in σ'_{ik} and R .

In the dissipationless limit ($\sigma' = R = 0$), the hydrodynamic equations are invariant with respect to the general coordinate transformations, provided that ρ , s , and v^i transform as

$$\delta \rho = -\xi^k \partial_k \rho, \quad (109)$$

$$\delta s = -\xi^k \partial_k s, \quad (110)$$

$$\delta v^i = -\xi^k \partial_k v^i + v^k \partial_k \xi^i + \dot{\xi}^i. \quad (111)$$

Now consider the dissipative terms. To keep the equations consistent with the diffeomorphism invariance, one must require that σ'_{ij} and R transform as a two-index tensor and a scalar, respectively:

$$\delta \sigma'_{ij} = -\xi^k \partial_k \sigma'_{ij} - \sigma_{kj} \partial_i \xi^k - \sigma_{ik} \partial_j \xi^k, \quad (112)$$

$$\delta R = -\xi^k \partial_k R. \quad (113)$$

In a flat space the viscous stress tensor is given by

$$\sigma'_{ij} = \eta (\partial_i v_j + \partial_j v_i) + \left(\zeta - \frac{2}{3} \eta \right) \delta_{ij} \partial_k v^k, \quad (114)$$

where η and ζ are the shear and bulk viscosities. In the naive extension to the curved space where one simply covariantizes the spatial derivatives, σ'_{ij} is not a pure two-index tensor; its variation under the diffeomorphism contains extra terms proportional to $\dot{\xi}^k$. The correct extension is

$$\sigma'_{ij} = \eta (\nabla_i v_j + \nabla_j v_i + \dot{g}_{ij}) + \left(\zeta - \frac{2}{3} \eta \right) g_{ij} \left(\nabla_k v^k + \frac{\dot{g}}{2g} \right). \quad (115)$$

Similarly, the dissipative function R in the curved space becomes

$$2R = \frac{\eta}{2} \left(\nabla_i v_j + \nabla_j v_i - \frac{2}{3} g_{ij} \nabla_k v^k + \dot{g}_{ij} - \frac{1}{3} g_{ij} \frac{\dot{g}}{g} \right)^2 + \zeta \left(\nabla_i v^i + \frac{\dot{g}}{2g} \right)^2 + \frac{\kappa}{T} \partial_i T \partial^i T. \quad (116)$$

We then turn to the conformal invariance. The dissipationless hydrodynamic equations are invariant under (104), if the dimensions of different fields are

$$\Delta[\rho] = 2\Delta[\psi] = 3, \quad \Delta[s] = 0, \quad \Delta[v^i] = 2. \quad (117)$$

Now let us consider the dissipation terms. From dimensional analysis, one finds that one has to set

$$\Delta[\eta] = \Delta[\zeta] = \Delta[\kappa] = \frac{3}{2} \quad (118)$$

for the hydrodynamic equations to be scale invariant. However, the conformal invariance is not preserved generically. The culprit is \dot{g}_{ij} that transforms as

$$\delta\dot{g}_{ij} = -\beta\ddot{g}_{ij} + \ddot{\beta}g_{ij}, \quad (119)$$

which leads to σ'_{ij} and R not to conform to the pattern of (104), unless the bulk viscosity ζ vanishes. Thus the requirement of the conformal invariance of the hydrodynamic equations implies $\zeta = 0$.

4.1.2 Superfluid phase

Similarly, we can repeat the argument for the superfluid case. The hydrodynamics of superfluids contains an additional degree of freedom, which is the condensate phase θ , whose gauge-covariant gradient is the superfluid velocity:

$$v_i^s = \frac{\hbar}{m}(\partial_i\theta + A_i). \quad (120)$$

It transforms in the same way as the normal velocity $v_i \equiv v_i^l$ under the general coordinate and conformal transformations. Its consequence is that the relative velocity between the superfluid and normal components $w^i = v_s^i - v^i$ transforms as a pure vector under the diffeomorphism:

$$\delta w^i = -\xi^k\partial_k w^i + w^k\partial_k \xi^i. \quad (121)$$

The $\dot{\xi}^i$ term in the variation cancels between δv_s and δv .

The diffeomorphism-invariant dissipative function in the curved space is

$$\begin{aligned} 2R = & \frac{\eta}{2} \left(\nabla_i v_j + \nabla_j v_i - \frac{2}{3}g_{ij}\nabla_k v^k + \dot{g}_{ij} - \frac{1}{3}g_{ij}\frac{\dot{g}}{g} \right)^2 \\ & + 2\zeta_1 \left(\nabla_i v^i + \frac{\dot{g}}{2g} \right) \nabla_j (\rho_s w^j) + \zeta_2 \left(\nabla_i v^i + \frac{\dot{g}}{2g} \right)^2 \\ & + \zeta_3 [\nabla_i (\rho_s w^i)]^2 + \frac{\kappa}{T} \partial_i T \partial^i T. \quad (122) \end{aligned}$$

Under the conformal transformations, R transforms as

$$\delta R = -\beta\dot{R} - \frac{7}{2}\dot{\beta}R + \frac{3}{2}\zeta_1\ddot{\beta}\nabla_i(\rho w^i) + \frac{3}{2}\zeta_2\ddot{\beta}\left(\nabla_i v^i + \frac{\dot{g}}{2g}\right). \quad (123)$$

The requirement of the conformal invariance of the superfluid hydrodynamics implies that the $\ddot{\beta}$ terms must have vanishing coefficients, i.e., $\zeta_1 = \zeta_2 = 0$.

In conclusion, we find that in the unitary limit, the bulk viscosity vanishes in the normal phase. In the superfluid phase, two of the three bulk viscosities vanish.

4.2 Superfluid effective field theory

At zero temperature, the long-distance dynamics of the unitary Fermi gas is described by an effective field theory, with some effective action S_{eff} . The effective theory should inherit the general coordinate invariance of the microscopic theory. This means that the effective action is invariant under the general coordinate transformations, which in its turn means that

$$\delta\mathcal{L} = -\xi^k\partial_k\mathcal{L}. \quad (124)$$

The low-energy degree of freedom is the phase of the condensate θ . The time reversal symmetry means that the effective theory is invariant under

$$t \rightarrow -t \quad \text{and} \quad \theta \rightarrow -\theta. \quad (125)$$

Since θ is a Nambu-Goldstone field, it should always appear with derivatives in the effective Lagrangian. Therefore, for power counting purposes, we can set $\dot{\theta}, \partial_i\theta \sim O(p^0)$. The leading-order effective Lagrangian should be

$$\mathcal{L} = \mathcal{L}(\dot{\theta}, \partial_i\theta, A_0, A_i, g_{ij}). \quad (126)$$

The gauge invariance and the invariance with respect to three-dimensional general coordinate transformations (with time-independent ξ^i) limit the Lagrangian to be a function of two variables:

$$\mathcal{L} = \mathcal{L}(D_t\theta, g^{ij}D_i\theta D_j\theta), \quad (127)$$

where

$$D_t\theta = \dot{\theta} - A_0 \quad \text{and} \quad D_i\theta = \partial_i\theta - A_i. \quad (128)$$

The invariance of the effective theory with respect to general coordinate transformations requires

$$\mathcal{L} = P(X) \quad \text{with} \quad X = D_t\theta - \frac{g^{ij}}{2m}D_i\theta D_j\theta. \quad (129)$$

If we now set the metric to be flat and the external field to be zero, we find the most general form of the Lagrangian for superfluids:

Table 5 Eight classes of scale invariant nonrelativistic systems proposed in Ref. [17]. In all cases below, the coupling of the interspecies contact interaction term has the dimension $[c_0] = -1$ and can be tuned to the nontrivial fixed point describing an interspecies resonance.

# of species and dimensions	Spatial configurations	Symmetries + M, D, C, H
2 species in pure 3D	$\mathbf{x}_A = \mathbf{x}_B = (x, y, z)$	P_i, K_i, J_{ij} with $i, j = x, y, z$
2 species in 2D-3D mixture	$\mathbf{x}_A = (x, y)$ $\mathbf{x}_B = (x, y, z)$	P_i, K_i, J_{ij} with $i, j = x, y$
2 species in 1D-3D mixture	$\mathbf{x}_A = (z)$ $\mathbf{x}_B = (x, y, z)$	P_z, K_z, J_{xy}
2 species in 2D-2D mixture	$\mathbf{x}_A = (x, z)$ $\mathbf{x}_B = (y, z)$	P_z, K_z
2 species in 1D-2D mixture	$\mathbf{x}_A = (z)$ $\mathbf{x}_B = (x, y)$	J_{xy}
3 species in 1D-1D-1D mixture	$\mathbf{x}_A = (x)$ $\mathbf{x}_B = (y)$ $\mathbf{x}_C = (z)$	None
3 species in 1D ² -2D mixture	$\mathbf{x}_A = \mathbf{x}_B = (x)$ $\mathbf{x}_C = (x, y)$	P_x, K_x
4 species in pure 1D	$\mathbf{x}_A = \mathbf{x}_B = \mathbf{x}_C = \mathbf{x}_D = (x)$	P_x, K_x

$$\mathcal{L} = P \left(\dot{\theta} - \frac{(\partial_t \theta)^2}{2m} \right), \quad (130)$$

which was previously found by Greiter, Wilczek, and Witten [35] using a different line of arguments. Moreover, by studying the thermodynamics of the effective theory one finds that the function $P(X)$ is the same function that determines the dependence of the pressure on the chemical potential.

To the next-to-leading order, the effective Lagrangian contains terms with two additional derivatives. The symmetries restrict the number of independent terms in the Lagrangian to two. This allows one to relate different physical quantities with each other [13].

5 Other scale and conformal invariant systems

We have discussed various theoretical aspects of the unitary Fermi gas. Finally we conclude this chapter by introducing other systems exhibiting the nonrelativistic scaling and conformal symmetries, to which a part of above results can be applied. One such system is a mass-imbalanced Fermi gas with both two-body and three-body resonances, which is already mentioned in Sect. 3.3.2. Its many-body physics is studied in Ref. [16].

The other systems are multi-species Fermi gases in mixed dimensions [17]. In all systems listed in Table 5, the coupling of the contact interaction term that involves all species has the dimension $[c_0] = -1$ and thus the theory with such an interaction term is renormalizable. In particular, when the coupling c_0 is tuned to its nontrivial fixed point ($c_0 \neq 0$) that describes an interspecies resonance, the resulting system becomes scale invariant. We can derive the reduced Schrödinger algebra and the operator-state correspondence for such a system [36]. The few-body and many-body physics of multi-species Fermi gases in mixed dimensions are studied in Refs. [17,

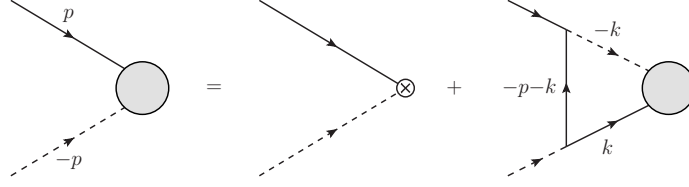


Fig. 15 Feynman diagrams to renormalize three-body composite operators. The solid lines are the propagators of ψ_\uparrow and ψ_\downarrow fields while the dotted lines are the resummed propagators of ϕ field. The shaded bulbs represent the vertex function $Z(p)$.

36, 37, 38, 39]. Some of these systems can be in principle realized in ultracold atom experiments. Indeed the 2D-3D mixture has been recently realized using ^{41}K and ^{87}Rb and the interspecies scattering resonances were observed [40].

6 Appendix: scaling dimensions of three-body operators

In this Appendix, we derive the formula to compute the scaling dimensions of three-body composite operators for arbitrary mass ratio m_\uparrow/m_\downarrow , angular momentum l , and spatial dimension d from a field theory perspective. We first consider a three-body operator composed of two spin- \uparrow and one spin- \downarrow fermions with zero orbital angular momentum $l = 0$:

$$\mathcal{O}_{\uparrow\uparrow\downarrow}^{(l=0)}(\mathbf{x}) \equiv Z_\Lambda^{-1} \phi \psi_\uparrow(\mathbf{x}), \quad (131)$$

where Z_Λ is a cutoff-dependent renormalization factor. We study the renormalization of the composite operator $\phi \psi_\uparrow$ by evaluating its matrix element $\langle 0 | \phi \psi_\uparrow(\mathbf{x}) | p, -p \rangle$. Feynman diagrams to renormalize $\phi \psi_\uparrow$ is depicted in Fig. 15. The vertex function $Z(p_0, \mathbf{p})$ in Fig. 15 satisfies the following integral equation:

$$\begin{aligned} Z(p_0, \mathbf{p}) &= 1 - i \int \frac{dk_0 d\mathbf{k}}{(2\pi)^{d+1}} G_\uparrow(k) G_\downarrow(-p-k) D(-k) Z(k_0, \mathbf{k}) \\ &= 1 - \int \frac{d\mathbf{k}}{(2\pi)^d} G_\downarrow(-p-k) D(-k) Z(k_0, \mathbf{k}) \Big|_{k_0 = \frac{\mathbf{k}^2}{2m_\uparrow}}, \end{aligned} \quad (132)$$

where we used the analyticity of $Z(k_0, \mathbf{k})$ on the lower half plane of k_0 . $G_\sigma(p) \equiv \left(p_0 - \frac{\mathbf{p}^2}{2m_\sigma} + 0^+\right)^{-1}$ is the fermion propagator and $D(p)$ is the resummed propagator of ϕ field given in Eq. (78). If we set $p_0 = \frac{\mathbf{p}^2}{2m_\uparrow}$, Eq. (132) reduces to the integral equation for $z(\mathbf{p}) \equiv Z\left(\frac{\mathbf{p}^2}{2m_\uparrow}, \mathbf{p}\right)$.

Because of the scale and rotational invariance of the system, we can assume the form of $z(\mathbf{p})$ to be $z(\mathbf{p}) \propto \left(\frac{|\mathbf{p}|}{\Lambda}\right)^\gamma$, where Λ is a momentum cutoff. Accordingly

the renormalization factor becomes $Z_\Lambda \propto \Lambda^{-\gamma}$ with $\gamma = -\partial \ln Z_\Lambda / \partial \ln \Lambda$ being the anomalous dimension of the composite operator $\phi \psi_\uparrow$. In terms of γ , the scaling dimension of the renormalized operator $\mathcal{O}_{\uparrow\downarrow}^{(l=0)}$ is given by

$$\Delta_{\uparrow\downarrow}^{(l=0)} = \Delta_\phi + \Delta_{\psi_\uparrow} + \gamma = 2 + \frac{d}{2} + \gamma. \quad (133)$$

Substituting the expression of $z(\mathbf{p})$ into Eq. (132) and performing the integration over $|\mathbf{k}|$ at $\Lambda \rightarrow \infty$, we obtain the following equation to determine γ :

$$1 = \frac{2\pi^{1/2} \left[\frac{m_\downarrow(2m_\uparrow+m_\downarrow)}{(m_\uparrow+m_\downarrow)^2} \right]^{1-d/2}}{\Gamma(1-\frac{d}{2}) \Gamma(\frac{d-1}{2}) \sin[(\gamma+1)\pi]} \int_0^\pi d\theta \sin^{d-2} \theta \frac{\sin[(\gamma+1)\chi]}{\sin \chi} \quad (134)$$

with $\cos \chi \equiv \frac{m_\uparrow}{m_\uparrow+m_\downarrow} \cos \theta$. The integration over θ can be done analytically in $d = 3$, but otherwise, has to be done numerically.

Similarly, for general orbital angular momentum l , we can derive the equation satisfied by the anomalous dimension γ_l :

$$1 = \frac{2\pi^{1/2} \left[\frac{m_\downarrow(2m_\uparrow+m_\downarrow)}{(m_\uparrow+m_\downarrow)^2} \right]^{1-d/2}}{\Gamma(1-\frac{d}{2}) \Gamma(\frac{d-1}{2}) \sin[(\gamma+l+1)\pi]} \int_0^\pi d\theta \sin^{d-2} \theta \tilde{P}_l(\cos \theta) \frac{\sin[(\gamma+l+1)\chi]}{\sin \chi}, \quad (135)$$

where $\tilde{P}_l(z)$ is a Legendre polynomial generalized to d spatial dimensions.⁷ The scaling dimension of the renormalized operator $\mathcal{O}_{\uparrow\downarrow}^{(l)}$ with orbital angular momentum l is now given by

$$\Delta_{\uparrow\downarrow}^{(l)} = \Delta_\phi + \Delta_{\psi_\uparrow} + l + \gamma_l = 2 + \frac{d}{2} + l + \gamma_l. \quad (136)$$

$\Delta_{\uparrow\downarrow}^{(l)}$ for $l = 0, 1$ in $d = 3$ are plotted as functions of the mass ratio m_\uparrow/m_\downarrow in Fig. 12, while $\Delta_{\uparrow\downarrow}^{(l)}$ for $l = 0, 1$ with equal masses $m_\uparrow = m_\downarrow$ are plotted in Fig. 14 as functions of the spatial dimension d .

References

1. C. A. Regal, M. Greiner, and D. S. Jin, ‘‘Observation of Resonance Condensation of Fermionic Atom Pairs,’’ *Phys. Rev. Lett.* **92**, 040403 (2004) [arXiv:cond-mat/0401554].
2. M. W. Zwierlein, C. A. Stan, C. H. Schunck, S. M. F. Raupach, A. J. Kerman, and W. Ketterle, ‘‘Condensation of Pairs of Fermionic Atoms near a Feshbach Resonance,’’ *Phys. Rev. Lett.* **92**, 120403 (2004) [arXiv:cond-mat/0403049].
3. D. M. Eagles, ‘‘Possible pairing without superconductivity at low carrier concentration in bulk and thin-film superconducting semiconductors,’’ *Phys. Rev.* **186**, 456 (1969).

⁷ $\tilde{P}_0(z) = 1$, $\tilde{P}_1(z) = z$, ...

4. A. J. Leggett, in *Modern Trends in the Theory of Condensed Matter*, edited by A. Pekalski and R. Przystawa (Springer-Verlag, Berlin, 1980); J. Phys. (Paris), Colloq. **41**, C7-19 (1980).
5. P. Nozières and S. Schmitt-Rink, “Bose condensation in an attractive fermion gas: from weak to strong coupling superconductivity,” J. Low Temp. Phys. **59**, 195 (1985).
6. Y. Nishida and D. T. Son, “ ϵ expansion for a Fermi gas at infinite scattering length,” Phys. Rev. Lett. **97**, 050403 (2006) [arXiv:cond-mat/0604500].
7. Y. Nishida and D. T. Son, “Fermi gas near unitarity around four and two spatial dimensions,” Phys. Rev. A **75**, 063617 (2007) [arXiv:cond-mat/0607835].
8. Y. Nishida, “Unitary Fermi gas at finite temperature in the ϵ expansion,” Phys. Rev. A **75**, 063618 (2007) [arXiv:cond-mat/0608321].
9. P. Arnold, J. E. Drut, and D. T. Son, “Next-to-next-to-leading-order ϵ expansion for a Fermi gas at infinite scattering length,” Phys. Rev. A **75**, 043605 (2007) [arXiv:cond-mat/0608477].
10. Y. Nishida, “Ground-state energy of the unitary Fermi gas from the ϵ expansion,” Phys. Rev. A **79**, 013627 (2009) [arXiv:0808.3826 [cond-mat.other]].
11. Y. Nishida and D. T. Son, “Nonrelativistic conformal field theories,” Phys. Rev. D **76**, 086004 (2007) [arXiv:0706.3746 [hep-th]].
12. D. T. Son, “Vanishing bulk viscosities and conformal invariance of unitary Fermi gas,” Phys. Rev. Lett. **98**, 020604 (2007) [arXiv:cond-mat/0511721].
13. D. T. Son and M. Wingate, “General coordinate invariance and conformal invariance in nonrelativistic physics: Unitary Fermi gas,” Annals Phys. **321**, 197 (2006) [arXiv:cond-mat/0509786].
14. C. R. Hagen, “Scale and conformal transformations in galilean-covariant field theory,” Phys. Rev. D **5**, 377 (1972).
15. U. Niederer, “The maximal kinematical invariance group of the free Schrödinger equation,” Helv. Phys. Acta **45**, 802 (1972).
16. Y. Nishida, D. T. Son, and S. Tan, “Universal Fermi Gas with Two- and Three-Body Resonances,” Phys. Rev. Lett. **100**, 090405 (2008) [arXiv:0711.1562 [cond-mat.other]].
17. Y. Nishida and S. Tan, “Universal Fermi gases in mixed dimensions,” Phys. Rev. Lett. **101**, 170401 (2008) [arXiv:0806.2668 [cond-mat.other]].
18. Z. Nussinov and S. Nussinov, “Triviality of the BCS-BEC crossover in extended dimensions: Implications for the ground state energy,” Phys. Rev. A **74**, 053622 (2006) [arXiv:cond-mat/0410597].
19. Y. Nishida, “Unitary Fermi gas in the ϵ expansion,” Ph.D. Thesis, University of Tokyo, 2007 [arXiv:cond-mat/0703465].
20. S. Zhang, K. E. Schmidt, and J. Carlson, private communication.
21. P. Nikolic and S. Sachdev, “Renormalization-group fixed points, universal phase diagram, and $1/N$ expansion for quantum liquids with interactions near the unitarity limit,” Phys. Rev. A **75**, 033608 (2007) [arXiv:cond-mat/0609106].
22. J. Carlson and S. Reddy, “Asymmetric Two-component Fermion Systems in Strong Coupling,” Phys. Rev. Lett. **95**, 060401 (2005) [arXiv:cond-mat/0503256].
23. E. Burovski, N. Prokof’ev, B. Svistunov, and M. Troyer, “Critical Temperature And Thermodynamics Of Attractive Fermions At Unitarity,” Phys. Rev. Lett. **96**, 160402 (2006) [arXiv:cond-mat/0602224].
24. M. Henkel, “Schrödinger invariance in strongly anisotropic critical systems,” J. Statist. Phys. **75**, 1023 (1994) [arXiv:hep-th/9310081].
25. F. Werner and Y. Castin, “The unitary three-body problem in a trap,” Phys. Rev. Lett. **97**, 150401 (2006) [arXiv:cond-mat/0507399];
F. Werner and Y. Castin, “The unitary gas in an isotropic harmonic trap: symmetry properties and applications,” Phys. Rev. A **74**, 053604 (2006) [arXiv:cond-mat/0607821].
26. S. Tan, “Short Range Scaling Laws of Quantum Gases With Contact Interactions,” arXiv:cond-mat/0412764.
27. Y. Tachikawa, private communication.
28. C. A. Bertulani, H. W. Hammer, and U. Van Kolck, “Effective Field Theory for Halo Nuclei,” Nucl. Phys. A **712**, 37 (2002) [arXiv:nucl-th/0205063].

29. H. W. Hammer and D. Lee, "Causality and universality in low-energy quantum scattering," *Phys. Lett. B* **681**, 500 (2009) [arXiv:0907.1763 [nucl-th]];
H. W. Hammer and D. Lee, "Causality and the effective range expansion," arXiv:1002.4603 [nucl-th].
30. T. Busch, B.-G. Englert, K. Rzażewski, and M. Wilkens, "Two Cold Atoms in a Harmonic Trap," *Found. Phys.* **28**, 549 (1998).
31. T. Stöferle, H. Moritz, K. Günter, M. Köhl, and T. Esslinger, "Molecules of Fermionic Atoms in an Optical Lattice," *Phys. Rev. Lett.* **96**, 030401 (2006) [arXiv:cond-mat/0509211].
32. V. Efimov, "Level Spectrum of Three Resonantly Interacting Particles," *Sov. Phys. JETP Lett.* **16**, 34 (1972);
V. Efimov, "Energy levels of three resonantly interacting particles," *Nucl. Phys. A* **210**, 157 (1973).
33. D. Blume, J. von Stecher, and C. H. Greene, "Universal Properties of a Trapped Two-Component Fermi Gas at Unitarity," *Phys. Rev. Lett.* **99**, 233201 (2007) [arXiv:0708.2734 [cond-mat.other]].
34. Y. Castin, "Exact scaling transform for a unitary quantum gas in a time dependent harmonic potential," *Comptes Rendues Physique* **5**, 407 (2004) [arXiv:cond-mat/0406020].
35. M. Greiter, F. Wilczek, and E. Witten, "Hydrodynamic Relations In Superconductivity," *Mod. Phys. Lett. B* **3**, 903 (1989).
36. Y. Nishida, "Induced p -wave superfluidity in two dimensions: Brane world in cold atoms and nonrelativistic defect CFTs," *Annals Phys.* **324**, 897 (2009) [arXiv:0810.1321 [cond-mat.other]].
37. Y. Nishida and S. Tan, "Confinement-induced Efimov resonances in Fermi-Fermi mixtures," *Phys. Rev. A* **79**, 060701 (2009) [arXiv:0903.3633 [cond-mat.other]].
38. Y. Nishida, "Phases of a bilayer Fermi gas," arXiv:0906.4584 [cond-mat.quant-gas].
39. Y. Nishida and D. T. Son, "Universal Four-Component Fermi Gas in One Dimension," arXiv:0908.2159 [cond-mat.quant-gas].
40. G. Lamporesi, J. Catani, G. Barontini, Y. Nishida, M. Inguscio, and F. Minardi, "Scattering in mixed dimensions with ultracold gases," *Phys. Rev. Lett.* **104**, 153202 (2010) [arXiv:1002.0114 [cond-mat.quant-gas]].